Payload Concepts for Investigations of Electrostatic Dust Motion on the Lunar Surface

Christine M. Hartzell[a,*], Paul Bellan[e], Dennis Bodewits[b], Gian Luca Delzanno[g], Masatoshi Hirabayashi[c], Truell Hyde[d], Uwe Konopka[b], Edward Thomas, Jr.[b], Hubertus M. Thomas[f], Inseob Hahn[h], Ulf Israelsson[h]

[a] *Department of Aerospace Engineering, University of Maryland, College Park, MD*
[b] *Department of Physics, Auburn University, Auburn, AL*
[c] *Department of Aerospace Engineering, Auburn University, Auburn, AL*
[d] *Department of Physics, Baylor University, Waco, TX*
[e] *Department of Physics, California Institute of Technology, Pasadena, CA*
[f] *Institut für Materialphysik im Weltraum, Deutsches Zentrum für Luft- und Raumfahrt (DLR), Weßling, Germany*
[g] *Los Alamos National Laboratory, Los Alamos, NM*
[h] *Jet Propulsion Laboratory, California Institute of Technology, Pasadena, CA*

Abstract

Significant experimental and computational investigations have explored the feasibility of electrostatically-motivated dust motion on the lunar surface. The motion of lunar dust influences our understanding of the evolution of the surface and may also present a hazard to future exploration vehicles and astronauts. The possibility of a sustained exploration presence on the lunar surface opens the door to long-term experiments on the lunar surface, akin to the science facilities on the International Space Station. We have identified four measurements/observations that would significantly advance our understanding of dust-plasma interactions on the lunar surface. In this context, we provide conceptual designs for payloads to obtain these observations: a Langmuir probe, dust deposit witness plate, regolith charge measurement instrument, and cameras to look for evidence of horizon glow. These payloads could deploy independently and sequentially, or together as a suite. The proposed payloads would provide key observations that would inform future modeling efforts and direct future in

*Corresponding author
Email address: hartzell@umd.edu (Christine M. Hartzell)

situ experiments to understand the dust-plasma environment, both for planetary science and spacecraft design applications.

Keywords: electrostatic, regolith, Lunar surface

1. Introduction

Electrostatically-motivated dust motion has been hypothesized since the Lunar Horizon Glow was observed by the Surveyor spacecraft [1]. The Lunar Horizon Glow was an unexpected brightness above the horizon observed after sunset thought to be caused by forward scattering of light off of $\sim 5\mu$m particles hovering tens of cm above the lunar surface. It was hypothesized that regolith particles detached from the surface and possibly levitated there due to electrostatic forces produced by interactions with the solar wind plasma.

In addition to the Horizon Glow observations, results of the Lunar Ejecta and Micrometeorite (LEAM) experiment, placed on the surface during the Apollo 17 mission, have been interpreted as the re-impact of electrostatically lofted dust [2]. Additionally, dust accumulation has been proposed as a cause of the observed long-term degradation in the efficiency of retroreflectors on the lunar surface [3]. However, recent reanalysis of Apollo Horizon Glow observations attributed the observed light to zodiacal light [4]. Additionally, dust detected by the recent Lunar Dust Experiment (LDEX) instrument on the LADEE mission is thought to have been produced by micrometeoroid bombardment and no evidence of electrostatically-motivated dust motion was observed at 20-100 km altitude above the lunar surface [5, 6]. Thus, no conclusive observational evidence of electrostatically-motivated dust motion on the Moon exists. However, the feasibility of electrostatic lofting and levitation has been proven computationally [7, 8, 9] and experimentally [10, 11, 12]. Thus, the in situ feasibility of this phenomenon remains of interest due to its potential implications for the evolution of the lunar surface as well as operations of exploration vehicles and astronaut safety.

The solar wind plasma interacts directly with the lunar regolith, which con-

tains angular particles down to nanometer-scale in size. Additionally, solar UV radiation causes photoemission of the regolith. While photoemission typically causes the daylit surface of the Moon to have a net positive charge (unless the Moon is in the plasma sheet [13]), recent work [14, 15, 16] has shown that individual particles may have a net negative charge (achieved by collecting photoemitted electrons from neighboring particles). Additionally, particles on the lunar surface may accumulate charge via triboelectric charging during exploration operations (i.e., the 'static electricity' produced by particles rubbing or rolling over one another due, for instance, to a rover wheel's interaction with the surface [17]). Interactions of the charged surface with the solar wind result in the formation of a region of non-uniform plasma density near the surface called the plasma sheath. The non-uniform ion and electron densities in the plasma sheath result in an electric field. The electrostatic force on a particle is the product of the particle's charge and the local electric field. If the electrostatic force is larger than the gravity and cohesive forces holding the particle on the surface, the particle will detach [18, 10], a phenomenon called electrostatic lofting. Electrostatic lofting may be a naturally occurring phenomenon and it could also be enhanced by exploration activities: for example, rover-induced tribocharging or spacecraft shadows (causing stronger local electric fields) may induce electrostatic lofting.

In addition to electrostatic lofting, it is possible for regolith to detach from the lunar surface due to micrometeorite impacts or exploration activities. Because all regolith particles are charged, these detached particles will also experience an electrostatic force. Under certain conditions, the electrostatic force is predicted to oppose gravity [19]. Thus, particles launched with a specific range of initial conditions may hover above the surface, a phenomenon called electrostatic levitation. Electrostatic levitation may influence the transport of regolith across the lunar surface, the deposition of dust on spacecraft surfaces and may obscure observations made from the lunar surface. Note that electrostatic lofting and levitation are independent phenomena, both caused by the interaction of charged lunar dust with the plasma environment.

Electrostatically-motivated dust motion on the lunar surface is relevant to planetary scientists, mission designers and technologists. If active on the lunar surface, electrostatic dust motion provides a mechanism to redistribute small particles across the surface. Additionally, if electrostatic dust motion is active on the Moon, then it is also likely to be an active process on other airless planetary bodies (e.g., asteroids [20] and moons), potentially influencing rates of resurfacing on these bodies. Electrostatically-motivated dust motion presents both a hazard and opportunity to surface exploration vehicles. Lofted dust may obscure observations and its deposition on spacecraft surfaces may impair the function of solar panels and change the thermal properties of spacecraft. However, the ability to move small particles via electrostatic forces may also enable new dust clearing and sample collection technologies. Methods to clear dust from surfaces using electrostatic forces are discussed in our companion paper [21].

The planned increase in lunar surface exploration activities presents a unique opportunity to look for evidence of electrostatically-motivated dust motion and measure properties of the local plasma environment that would drive these phenomena. Human or long-term surface exploration missions are particularly attractive to investigations of these phenomena because they enable measurements at a variety of conditions (e.g. altitudes, time of day, and locations). For example, it is necessary to measure the plasma densities at different altitudes in order to derive the plasma sheath structure, which dictates the altitudes at which electrostatic levitation would be predicted and the size of particles capable of stable levitation. The plasma properties are also highly sensitive to the time of day and local topography, as the presence of shadows significantly influences the sheath structure. Additionally, a sustained exploration presence on the lunar surface would enable long-term, multi-investigator facilities on the lunar surface akin to the laboratory facilities present on the ISS [22]. Multi-investigator facilities would enable a series of experiments to tease apart the physics that produces electrostatically-motivated dust motion on the lunar surface.

We present conceptual designs for four investigations to look for evidence of

and measure the key physical quantities influencing electrostatically-motivated dust motion on the lunar surface. Measurements of the near-surface plasma environment are fundamental to assessing the feasibility of and modeling electrostatic dust motion. We present a Langmuir probe specifically designed for the unique plasma properties of the lunar surface. The electric charge of individual dust grains on the lunar surface remains poorly constrained by both experimental and theoretical studies and we describe two possible instruments to provide these measurements. Looking for larger scale evidence for electrostatic dust phenomena, we present a dust coupon payload that would enable measurement of the rate of dust deposited on surfaces and camera systems specifically designed to detect the lunar horizon glow. These measurements would elevate the study of electrostatic phenomena from opportunistic to intentional, resulting in higher quality observations.

2. Measuring Lunar Near-Surface Plasma Properties with a Langmuir Probe

2.1. Motivation and Science Objectives

In order to characterize the feasibility of electrostatically-dominated dust motion on the Moon, it is necessary to understand the local plasma environment. The local plasma environment influences both the electrical charge of regolith particles as well as the local electric field. The primary plasma parameters of interest are the densities and temperatures of the electrons and ions. The ion and electron temperatures, T_i and T_e, will be unequal. Similarly, the electron and ion densities are unequal in the plasma sheath. Photoelectrons are also a significant species in the near-surface lunar plasma sheath and, under certain conditions, could dominate the electron density near the surface. A further complication is that, should there be a large density of small dust grains, the majority of photoelectrons would settle on the dust grains further reducing the density of free electrons n_e. The plasma environment on the day and night surfaces varies dramatically due to the lack of photoemission and presence of an ion

wake on the nightside. Existing estimates of plasma electron and ion densities span four orders of magnitude when different Moon charging regimes and model uncertainties are included. Existing estimates of the electron densities at the surface span $10^6 \mathrm{m}^{-3} = 1 \mathrm{cm}^{-3}$ (estimated from solar wind electrons in absence of photoemission) [7, 19] to $10^{11} \mathrm{m}^{-3} = 10^5 \mathrm{cm}^{-3}$ (in a photoemission-dominated regime, with large uncertainties on the photoemission yield) [23]. In order to reduce these uncertainties, it is therefore critical to measure the actual plasma parameters in situ.

Langmuir probes provide the simplest means for measuring $n_e, T_e,$ and n_i (ion density) in the expected parameter regime. The design of a Langmuir probe requires an initial estimate of the densities and temperatures expected. We will begin with models of the plasma environment.

2.2. The Non-Monotonic Photoelectron Sheath

Figure 1 shows the various processes and currents that influence the structure of the plasma sheath. We focus on a particular Moon charging regime; where the lunar surface is illuminated by sunlight, resulting in a non-monotonic sheath structure. UV light from the sun illuminates the lunar surface and causes the lunar surface to emit photo-electrons (blue curved and straight arrows). The emitted electrons form a cloud a few meters above the lunar surface where they produce a negative potential. Low energy solar wind electrons reflect from the repulsive potential of this negative cloud (yellow) while high energy solar wind electrons make it over the potential barrier to reach the lunar surface. Solar wind ions see the negative cloud as a potential valley but can be repelled by the positive potential of the lunar surface (see Figure 2). Only high energy solar wind ions reach the surface. Dust grains (green) located slightly above the lunar surface charge negatively by being impacted by electrons from the electron cloud; this competes with UV sunlight causing photo-electrons being emitted from the dust and causing positive charging. It is expected that the negative charging will dominate near the lunar surface so the equilibrium dust charge will be negative in the first few meters above the surface. From the work of

[19], this is true when θ, the angle of incidence of sunlight relative to the surface normal, is less than approximately 75° (the lunar surface potential is positive for $\theta \leq 65°$). At higher altitudes where there are far fewer electrons, the dust grains are charged positive as a result of photo-emission of electrons by the solar UV light. While this investigation focuses on nominal conditions, we note that the polarity of the lunar regolith and structure of the plasma sheath (i.e. monotonic or non-monotonic) also depends on the solar wind conditions (e.g., the density and temperature of the solar wind can change during coronal mass ejections or the passage of the Moon through the Earth' magnetotail) [24, 25].

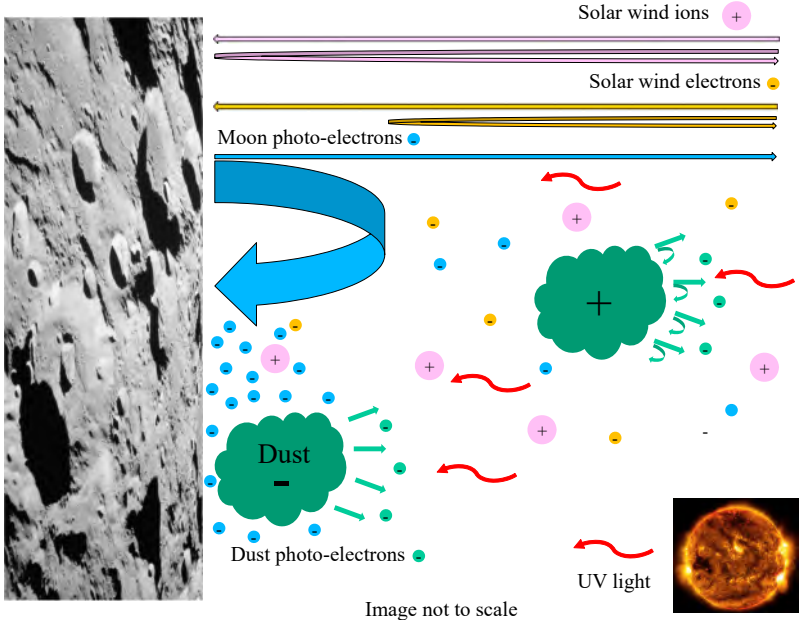

Figure 1: Sketch showing different processes that compete for a non-monotonic photoelectron sheath.

2.3. Modeling the Plasma Potential

We have developed a one-dimensional, kinetic, steady-state theory for the lunar sheath illuminated by the sun at normal incidence ($\theta = 0$). It includes

drifting Maxwellian solar wind electrons and ions and Maxwellian photoelectrons from the Moon's surface. The theory follows the work of Nitter et al. [19]. It uses conservation of energy to find the plasma distribution function of the various particle species at each altitude above the lunar surface, using the known source for those particles. The particle density is then expressed as a function of the local electrostatic potential and the resulting non-linear Poisson's equation is solved numerically. To do so, we have used floating potential boundary conditions on the Moon's surface and homogeneous Dirichlet boundary conditions at the other boundary of the computational domain, away from the Moon's surface. The parameters used in the simulations are those of Poppe and Horanyi [7]. Specifically, the density and temperature of the solar wind electrons are $n_{e,sw} \approx 10$ cm^{-3} and $T_{e,sw} = 10$ eV with a drift velocity of 400 km/s. The photoelectrons are emitted with a Maxwellian distribution function with current density equal to $J_{ph} = 4.5 \times 10^{-6}$ A/m^2 and temperature $T_{ph} = 2.2$ eV. The solar wind protons are treated by a cold (i.e. thermal velocity much smaller than drift velocity) drifting Maxwellian population with drift velocity equal to $v_{di,sw} = 400$ km/s. The ions are not modelled self-consistently. Rather, the solar wind ion density $n_{i,sw}$ is kept constant in the simulation domain and determined by imposing quasi-neutrality away from the lunar surface. The solar wind ion current density is $en_{i,sw}v_{di,sw}$. These approximations are valid since, for these parameters, the lunar surface charging is determined by the balance between the photoelectron flux and the solar wind electron flux, and the resulting sheath potential is of the order of the electron temperature, which is much smaller than the ion drift energy. Indeed, the simulation work of Poppe and Horanyi [7] shows that the solar wind density is essentially constant over the simulation domain for the parameters considered. The simulation domain is perpendicular to the lunar surface and extends from the lunar surface to 100 m.

Figure 2 plots the electrostatic potential in the domain, showing a non-monotonic behavior associated with the Moon's photoelectrons. These results are quite similar to those of Poppe and Horanyi [7] which were obtained with

Particle-In-Cell simulations. In our case the value of the electrostatic potential at 0.1 m altitude is ~ 4 V (versus ~ 3 V) and the minimum of the potential well is ~ -0.8 V (versus ~ -1.5 V) at about the same distance (~ 10 m). These results are also consistent with those of Nitter et al. [19] who showed that a non-monotonic sheath with positive surface potential forms for $\theta < 65°$. Figure 3 plots the densities of the photo-emitted electrons, the solar wind electrons, and the solar wind ions. For the parameters considered the electron density is dominated by the photoelectrons up to a distance of $\sim$10 m from the surface and the peak electron density is about 100 cm^{-3} (i.e., 10^8 m^{-3}). Once again these results are quite similar to those of Poppe and Horanyi [7]. We obtain an electron density of 1.1×10^8 m^{-3} (versus 1.5×10^8 m^{-3}) at the lunar surface and the system returns to quasi-neutrality at about 20 m altitude. At the lunar surface, the solar wind electron density is 2.4×10^6 m^{-3} (versus $\sim 2.0 \times 10^6$ m^{-3}) while at 100 m altitude it is 6.5×10^6 m^{-3} (versus $\sim 8 \times 10^6$ m^{-3} [7]).

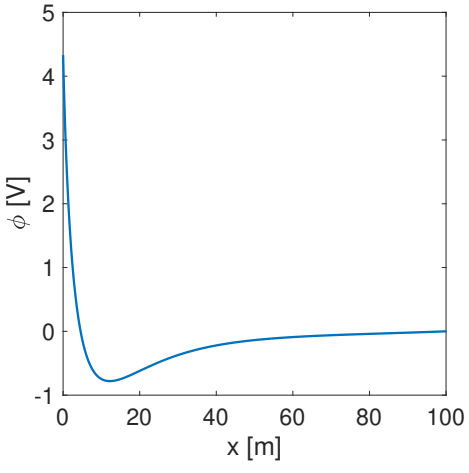

Figure 2: Electrostatic potential v. altitude.

Although the density of dust above the lunar surface is unknown, some constraints can be invoked to bound the dust density. These constraints are presented in Table 1. For reference, Kuznetsov et al. [26] and Popel et al. [23] presented a calculation predicting dust densities in the range of $10^2 - 10^3$

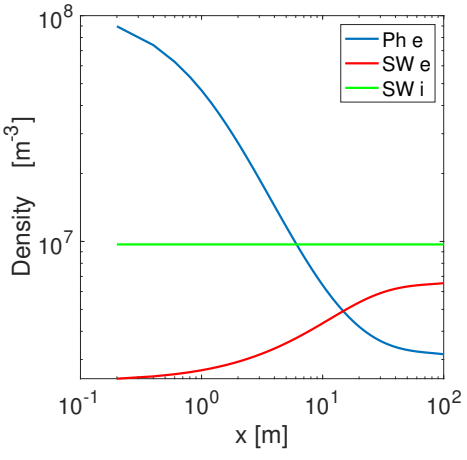

Figure 3: Electron and ion densities vs. altitude for photo-emitted electrons (Ph e), solar wind electrons (SW e), and solar wind ions (SW i).

cm^{-3} which is larger than the presumed electron density and so seems high. Another consideration is that dust charge is proportional to dust radius. The calculation presented assumes that the dust does not perturb the plasma and so corresponds to Regime 1 in Table 1. This non-perturbation assumption provides an upper limit on dust density as shown by Regime 2 in Table 1 for an example dust radius. Regime 3 in Table 1 describes a situation where all electrons reside on the dust grains so there are no free electrons.

2.4. Anticipated Plasma Parameters

In order to identify the range of parameters that are relevant to the Langmuir probe design, we summarize the results of the previous subsection. The model yields a non-monotonic lunar sheath dominated by the photoelectron density in the range 10-100 cm^{-3} up to $\sim$ 10 m altitude above the surface. The photoelectron temperature is 2.2 eV. This yields a current density of approximately 0.04-0.4 nA/cm^2 and a current of the order of 0.05-0.5 μA for the probe having 0.125 m^2 collection area (corresponding to the surface area of a 10 cm radius sphere). Note, however, that the photoelectron density estimates obtained by Popel et al. [23] are much higher (on the order of 10^5 cm^{-3}), giving a current

Table 1: Possible effects of dust on the near-surface plasma sheath. Regime 1 is based on the description in [7]. Regimes 2 and 3 impose limits on the dust density. Note that the dust charge depends linearly on the dust radius, hence the dust density estimates also depend on the dust radius. We have assumed a nominal dust radius of 0.1 μm for illustration purposes but the dust density estimates can be easily adapted to a different choice of the dust radius.

Regime	**Features**	**Notes**
1. No dust	$n_{e0} \approx n_i \sim 10^7 - 10^8$ m^{-3}	non-monotonic potential
	$T_{e,i} \sim 2 - 10$ eV	with minimum at ~ 10 m
2. Dust,	$n_{e0,i}, T_{e,i}$ same as Regime 1,	
but non-perturbing	dust density n_d must be	dust being nonperturbing is
	below a critical value	defined as dust charge density
	dependent on dust density,	less than 10% of larger of
	e.g., if $r_d = 0.1$ μm, $Q_d = 100e$,	electron or ion charge density
	then require $n_d < 10^4$ m^{-3}	
3. Dust,	$n_i \gg n_{e0}$ and $T_{e,i}$ as in Regime 1,	example:
strongly perturbing	almost no free electrons as	$r_d = 0.1$ μm,
	most electrons reside on dust	$Q_d = -1000e$, $n_d = 10^5$ m^{-3}
		so $n_i \simeq \lvert Q_d \rvert n_d \approx 10^8$ m^{-3} $\gg n_e$

of the order of 1 mA. The nature of the lunar sheath changes depending on the angle of incidence of sunlight relative to the surface normal, θ. As θ increases, the emitted photoelectron current density is reduced and eventually the surface becomes negatively charged and the sheath becomes a classic Debye sheath [19]. In the limit where $\theta = 90°$, no photoelectrons are emitted and the Debye sheath is completely determined by solar wind electrons and ions. If we assume a nominal 1 cm^{-3} solar wind electron density in the sheath, which is reduced relative to the nominal unperturbed solar wind density of $\sim$ 10 cm^{-3}, and a typical temperature of $T_e = 10$ eV, the electron current density is approximately 0.01 nA/cm^2 and the probe current is about 10 nA.

These modeled parameters represent a best guess, so it is prudent to design the probe so it can work in situations substantially different from this best guess, such as much higher/lower temperatures or densities. The densities and temperatures depend upon height above the lunar surface, whether it is lunar day or night, and on solar angle. Thus the Langmuir probe must be designed to measure time- and height-dependent densities in at least the range $10^6 - 10^{11}$ m^{-3} and time- and height-dependent temperatures in at least the range 2-20 eV. The estimated densities are at least a thousand times smaller than what is encountered in laboratory plasmas but are similar to those encountered in space plasmas. Estimated temperatures are similar to what is encountered in both space and laboratory plasmas. Expected scale lengths are more like those encountered in laboratory plasmas than in space plasmas. Thus, the design will differ from spacecraft Langmuir probes and from laboratory Langmuir probes while retaining some aspects of both. An additional issue is that photo-emission from the probe itself can create an electric current that, if not protected against, would confound the measurements and render them meaningless.

2.5. Langmuir Probe Fundamentals

A Langmuir probe consists of a sphere or cylinder that is electrically biased to either attract or repel electrons [27, 28]. The current I to the probe is measured as a function of the electric potential V applied to the probe. Analysis of this

current-potential relationship (called the I-V curve) enables the calculation of the plasma species densities and the local plasma potential denoted as V_p.

If $V = V_p$, the probe collects a reference electron current I_0 that is the product of the electron current density and the probe area $4\pi a^2$ where a is the radius of a spherical probe (the ion current, which is much smaller, is being neglected). This current I_0 is given by [28]

$$I_0 = \sqrt{8\pi} a^2 n_{e0} e \sqrt{\frac{\kappa T_e}{m_e}} \tag{1}$$

where n_{e0} is the unperturbed electron density away from the probe. I_0 results from all thermal electrons impacting the probe with neither impediment nor acceleration; here κ is Boltzmann's constant and m_e is the electron mass. In the repulsive mode, which is where $V - V_p$ is negative, a fraction of the electrons are repelled from the probe and the current is reduced from I_0 and now given by

$$I = I_0 \exp\left(\frac{e\,(V - V_p)}{\kappa T_e}\right). \tag{2}$$

In the attractive mode, which is where $V - V_p$ is positive, electrons are attracted to the probe and the current is increased from I_0 and now given by

$$I = I_0 \left(1 + \frac{e\,(V - V_p)}{\kappa T_e}\right)^{\alpha}. \tag{3}$$

The exponent α has the value $\alpha = 1$ for a sphere and $\alpha = 1/2$ for an infinite cylinder. By scanning V and measuring the resulting I, the transition from exponential behavior (repulsive) as given by Eqn 2 to the different behavior prescribed by Eqn 3 gives V_p. The slope of $\ln I$ plotted versus V when in repulsive mode gives T_e. The system must be able to measure a current about three orders of magnitude less than I_0 in order to resolve the slope of $\ln I$ versus V. Knowledge of T_e, of the probe dimensions, and the measured I_0 enables determination of n_e from Eqn 1.

If the probe is biased extremely negatively, it repels all the electrons. The ions fall into the probe sheath and a complex argument shows [29, 30] that the ion flux is that of ions at infinity coming in at the sound velocity which is

$\sqrt{\kappa T_e/m_i}$ where m_i is the ion mass. The ion saturation current (large negative bias on probe) is smaller than the electron saturation current by a factor of the order of $\sqrt{m_e/m_i}$ and can be used to give the ion density n_i. When there is dust, care must be taken to ensure that the dust does not confound the measurements.

2.6. Requirements

Based on the predicted characteristics of the near-surface plasma environment, we propose the following requirements for a Langmuir probe deployed from a landed lunar vehicle:

1. Be able to measure currents in the range 10 pA to 1 mA, based on estimates of n_e and T_e from the modeling (details in Section 2.4) as well as reasonable physical dimensions for the probe (discussed in this section). The lower limit is prescribed so as to provide accurate measurements of T_e.
2. Have a wide dynamic range for density, at least $1 - 10^5 \mathrm{cm}^{-3}$ from the discussion in Section 2.7.
3. Be moveable to different altitudes so as to obtain electric field and density profile
4. Not be affected by dust
5. Not be affected by photoemission from surfaces of the Langmuir probe and/or host spacecraft
6. Have a credible calibration using a known current source or a known plasma density

Additionally, as with all spacecraft instrumentation, it is desirable to minimize the mass and power requirements of the instrument.

2.7. Proposed design

The proposed design is shown in Figure 4 and will have a collection area of 0.125 m^2. Although a spherical shape was first considered, the need to avoid exposure to solar radiation [31] suggests that a cylindrical shape would be better.

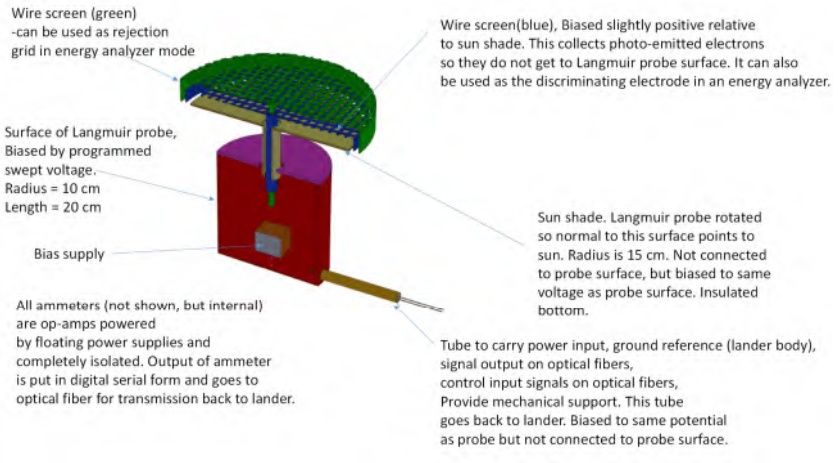

Figure 4: Physical layout of Langmuir probe. Electronics are inside the probe to avoid problems with cable capacitance and shielding.

The cylinder radius is 0.1 m and length is 0.2 m, a little bigger than a gallon of milk.

The nominal photoelectron current is 3 nA cm^{-2} (a midrange value from Whipple [32]). The nominal electron current density to a spherical probe is

$$J_e = n_{e0} e \sqrt{\frac{\kappa T_e}{2\pi m_e}} \tag{4}$$

equivalent to 0.01-10^3 nA/cm^2, assuming $T_e = 10$ eV and the electron density is in the range 1 cm^{-3} $< n_e <$ 10^5 cm^{-3} (see first paragraph of Section 2.4 for discussion of these parameters). Thus, the photoelectron current density can substantially exceed the expected electron saturation current density and so, for daytime measurements, a sunshade is required to block sunlight from reaching the Langmuir probe. The cylinder axis of the probe could then be continuously adjusted to point towards the sun so the probe will always be in

the sunshade shadow. A less expensive alternative would be to not have any adjustment and only use measurements that are made when the probe is in the shadow of the sunshade; this would greatly reduce the time when the probe is functional. The sunshade diameter is about 10% larger than the cylinder diameter and is electrically isolated from the probe but biased to the same potential as the probe. At very low plasma densities, photoemission caused by lunar illumination (reflected sunlight) off the Langmuir probe may exceed the current from the plasma. It may be necessary to have a "moonshield" below the Langmuir probe to reduce this small effect.

Two nearly transparent grids (middle, outer) with fine wires are located above the sunshade. The middle grid is biased slightly positive relative to the shield to collect all photo-emitted electrons so that these electrons do not circulate back to the Langmuir probe cylinder. The outer grid is also biased slightly positive. At night-time the sunshade and the two grids can be used as an energy analyzer for the solar wind plasma. The outer grid would then be biased to repel one species completely and the middle grid would have a variable repulsive bias for the other species to act as an energy analyzer. The powers involved in collecting currents from the probe and in biasing the sunshade are miniscule (order of picowatts to milliwatts) and will be dwarfed by the standby power required to operate the amplifiers and bias supplies.

To avoid collecting dust, the probe will be scanned at a frequency exceeding the dust plasma frequency [33]. This is not difficult since the dust plasma frequency is expected to be extremely low (less than 1 Hz). Note that we do not place strict requirements on the temporal resolution of the potential measurements as we seek to characterize the steady state plasma environment.

A ground reference and power cable (nominally 12 volts or some other standard) is supplied by the lunar lander. These cables enter the Langmuir probe body via a tube that goes back to the lander. The 12 volts is converted to approximately +100 volts and −100 volts that will be used to power the bias supply located inside the Langmuir probe cylindrical body. Having the bias supply inside the probe body rather than in the lander means there is no lengthy

cable going from the bias supply to the probe and so no cable capacitance to drive. Mitigating cable capacitance was a major issue discussed by Bose et al. [33] in a situation where the probe currents were larger and so less susceptible to this problem than here. The bias supply is controlled by a digital signal transmitted by an optical fiber from the lander.

Current is measured by floating operational amplifiers powered by supercapacitors/batteries recharged from the power cable using latching mechanical relays. The basic circuit for each ammeter is shown in Figure 5. The supercapacitors/batteries are physically disconnected from the lander supply by relays when the probe is operated so that each ammeter will be truly floating. As shown in Figure 6, there will be five ammeters to measure current at various locations in the circuit. This will enable cross-checking to see that the currents are consistent with each other by adding up appropriately. This cross-checking will be done on-board to provide quick results of verified density and temperature measurements but will also be recorded so that information can be gleaned from how these currents add up. The desired signal is the current from the Langmuir probe cylinder measured as a function of bias voltage.

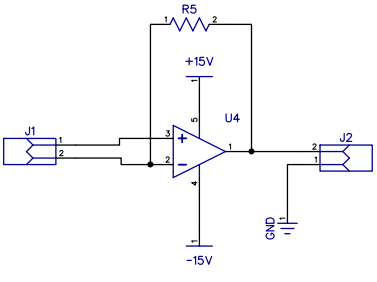

Figure 5: Simplified circuit of ammeter. The batteries powering this circuit will be floating. The output from J2 will be put in digital form and sent over optical fiber. Input of ammeter is J1.

Each ammeter consists of a floating operational amplifier operating in transconductance mode so the output voltage is IR where I is the current between the two input terminals and R is the feedback resistor. Because the operational

amplifier maintains a virtual ground, to an outside observer it would appear as if the non-inverting and inverting inputs are shorted together so the circuit functions as an ammeter. This operational amplifier output voltage is converted into a digital signal by an analog-to-digital converter and the digital signal is converted into a serial signal that is transmitted back to the lander over an optical fiber. Relays are used to switch in different values of feedback resistor R so as to have a high dynamic range. A one microampere current and a 1 megohm feedback resistor provide a 1 volt signal. Since electronic circuitry works well with signal levels from 10 millivolts to a few volts, use of a 1 megohm feedback resistor results in a 10 nanoamp current giving a 10 millivolt signal. A second stage might be used to provide picoamp sensitivity. Any substantial increase in sensitivity while maintaining acceptable signal to noise ratio could be used to reduce the physical size of the probe. Having sensitivity less than 10 picoamps is problematic because of electronics limitations. An optical fiber coming from the lander will carry signals that will be used to control the relays that switch in the battery charging and change the value of the feedback resistors.

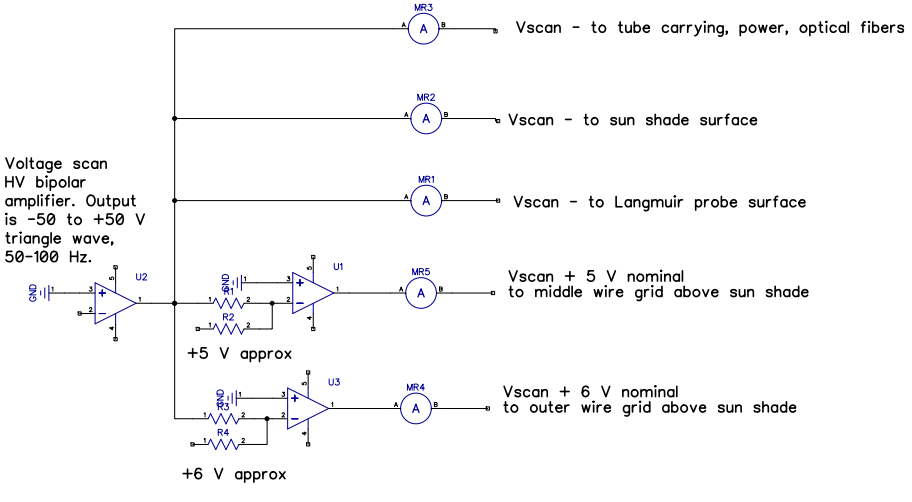

Figure 6: Circuit for bias probe parts and measuring current to each.

When the probe is at the local plasma potential, the current to the probe

changes from being exponentially dependent (Eqn 2) to depending on $(1 + eV/\kappa T)^{\alpha}$ (Eqn 3). Thus, the location of this transition in the I-V curve gives the local plasma potential. The magnitude of this current will give the electron density n_e using Eqn 1. The logarithmic dependence of the exponential region given by Eqn 2 will give the electron temperature T_e. The ion density n_i will be given by the ion saturation current (see [34] and Section 8.2.3 of [35], this calculation is more complicated in regimes where most electrons are on the dust grains). Dust will not be collected because the scan sweep frequency exceeds the dust plasma frequency so the dust only sees the time average of the sweep voltage. Based on the predicted dust charge, the voltage sweep can be designed so that it does not attract dust. Additionally, it may be possible to apply a quickly varying voltage to the probe in order to repel dust that has accumulated on the probe during a quiescent state, mimicking the operation of electrodynamic dust shields [36].

In terms of operation modes, the basic mode is to scan the bias voltage and measure the resulting current. It would be simple to conduct this scan at different speeds, hold the voltage at some specific level, or vary the voltages applied to the sunshield grids. These variations in the operations could enable the instrument to be tuned to specific space weather and illumination conditions.

Near the Langmuir probe, the tube carrying power cables and optical fibers will be at the Langmuir probe potential but then at some distance this will change to be at ground potential. The goal is to have all components near the Langmuir probe be at or near the Langmuir probe potential so this is the only potential seen by the plasma particles. The change to ground should be at a distance that is many times larger than the probe dimensions so that near the probe, the potential is not distorted. The sunshade blocks out the sun so there is no photoemission from the Langmuir probe. The current measured by the Langmuir probe ammeter is thus not confounded with photoemission current.

Electric field is proportional to the gradient in electric potential. Measurements of the electric field are key in refining predictions of the effect of electrostatic forces on the near-surface transport of dust. Thus, it is necessary

to characterize the plasma environment (densities and potentials) at multiple heights above the lunar surface. We envision that an arm or boom will be used to hold the Langmuir probe payload at varying altitudes above the surface. Additionally, because the spacecraft itself will modify the local plasma environment, it is necessary for the probe to be at least one Debye length away from the spacecraft during operation. The arm and probe must also be oriented so that the probe is not downwind (or in the shadow) of the spacecraft. No attempt has been made to design this arm as it is presumed that this will borrow heavily from heritage designs. It is presumed that this arm will move the probe from being just above the surface (since the dimension of the probe is 0.2 m, this would be the minimum altitude) to a height of at least 2 meters and possibly as much as 10 meters. The spatial resolution should be at least 0.5 m. An alternative to a moveable arm would be erection of a tall tower from which the probe would be suspended and then raised to various altitudes. These heights are determined by the electron Debye length which is the natural scale length of the system and can be expressed as

$$\begin{aligned} \lambda_D &= \sqrt{\frac{\varepsilon_0 \kappa T_e}{n_e q_e^2}} \\ &= 7.4 \times \left(\frac{T_e}{10 \text{ eV}}\right)^{1/2} \times \left(\frac{10^7 \text{ m}^{-3}}{n_e}\right)^{1/2} \text{ m.} \end{aligned} \tag{5}$$

The distance over which the potential changes is of the order of several Debye lengths and so it would be desirable to resolve several Debye lengths. This is an ambiguous requirement because it depends on the electron density, the unknown parameter which is the main goal of the measurement. The temperature is assumed to be 5-10 eV. If the density is set to be the lowest value considered in Section 2.4, namely $n = 10^6$ m^{-3} $= 1$ cm^{-3}, then $\lambda_d = 23$ m while if the density is set to be the highest value from the model in Section 2.4, namely $n = 10^8$ m^{-3} $= 100$ cm^{-3} then $\lambda_d = 2.3$ m. However, if the density is set to be $n = 10^{11}$ m^{-3} $= 10^5$ cm^{-3} as was proposed in a model given in [23] then $\lambda_D = 0.07$ m; this value seems too small to allow the possibility of lofting or levitation as the electric field would be negligible at heights exceeding several

Table 2: Mass and power estimates

	Mass	**Power**
Probe cylinder	0.5 kg	n/a
Sunshields	0.2 kg	n/a
Bias supply	0.3 kg	2 W (steady)
Ammeters (4)	0.2 kg	1 W
Sun-pointing system	0.2 kg	1 W

λ_D. As discussed in Section 2.4, the height profiles of the potential and density can be quite complicated as they are determined by a competition between solar wind electrons coming towards the lunar surface and photo-emitted electrons leaving the lunar surface. As an additional complication, the photo-emitted flux depends on the cosine of the angle between the direction to the sun and the normal to the surface so glancing sunlight produces far fewer photo-electrons than head-on sunlight. As shown in [19], this angle dependence can radically change the shape of the electrostatic potential profile, but the scale of this shape is of the order of 5-10 Debye lengths.

2.8. Estimated System Requirements

The TRL of the system is estimated to be 4; Langmuir probes have been used for over half a century on spacecraft, but the design proposed here is somewhat different from what has been done before. Because of the qualitative nature of the design, weight and power requirements can only be estimated based on past experience. These estimates are given in Table 2.

2.9. Comparison with Prior Designs

Manju et al. [37] describe a much simpler Langmuir probe designed for the Chandrayaan-2 Lunar Lander, which was launched by India in 2019, but unfortunately crashed into the Moon during its landing attempt. The probe consisted of a 5 cm diameter sphere with electronics capable of collecting currents as low as 25 picoamps and as high as 25 microamps. The electronics were located

on the lander and the probe was mounted on a 1 meter boom. There was no provision for shielding sunlight to avoid emission of photoelectrons.

Kuznetsov et al. [26] describe a much simpler Langmuir probe designed for the Luna Golub Lunar Lander to be launched by Russia. The design is a cone a few cm in diameter with wires going back to the spacecraft. Calculations of floating potential were given in Kuznetsov et al. [38], but no calculations of anticipated currents were provided. A numerical simulation indicated that the probe should not be located closer than 1m to the lander.

3. In Situ Measurements of Lunar Dust Charge

Dust particles on or near the lunar surface are charged via interaction with the solar wind plasma, emission of photoelectrons and accumulation of photoelectrons emitted from nearby particles and the lunar surface. Measurements of the charge of undisturbed dust particles (at rest on the lunar surface) as well as particles that have been detached (via electrostatic lofting, micrometeoroid bombardment or other mechanisms) are necessary to predict regolith behavior. We begin this section by reviewing the electrostatic charging of dust particles.

3.1. Dust Charging Theory

The sheath electron and ion densities discussed in Section 2 have been used as input for a calculation of the equilibrium floating potential on an individual, spherical dust grain located in the lunar sheath. This is done in the framework of the orbital motion limited (OML) theory [27]. The calculation is based on the collection of lunar sheath photoelectrons, solar wind electrons and ions, as well as photoemission from the dust grain. The results are plotted in Figure 7 showing the dust floating potential at various distances above the lunar surface. The dust charge is directly proportional to the dust floating potential through the dust capacitance.

The results of Figure 7 highlight different charging regimes. In all cases, charging equilibrium is based on the balance between electron collection and

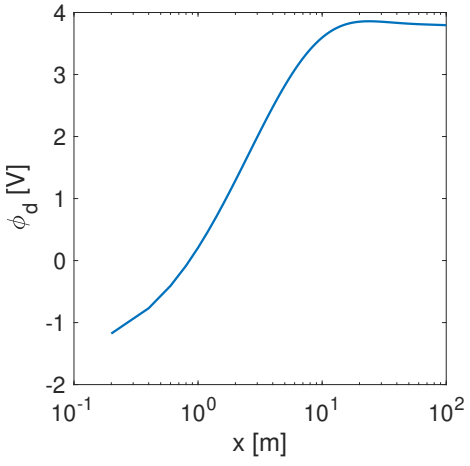

Figure 7: Dust floating potential as a function of altitude.

dust photoemission, with the collection of solar wind ions being negligible. Very close to the lunar surface, the high-density of lunar photoelectrons leads to negatively charged grains. At larger distances ($x >\sim 1$ m), the lunar photoelectron density decreases and equilibrium is established with the grains being positively charged. Note that these results are in good agreement with those of [7] who showed negatively charged dust grains near the lunar surface becoming positively charged away from the surface. Near the lunar surface [7] had ~ -1.3 V at 0.2 m altitude which compares well with our result of -1.2 V, while away from the lunar surface [7] had a dust potential around ~ 3.2 V while we have ~ 3.8 V. Our results are also consistent with those of [19], Fig. 3b.

For a dust radius of 0.1 μm, the dust floating potential in Figure 7 corresponds to a dust charge that ranges from $\sim -100e^-$ at the lunar surface to $\sim 264e^-$ at 100m away from the surface. The calculation presented in Figure 7 is based on OML which assumes that electrons and ions constitute a continuous fluid, i.e., particle discreteness is not taken into account. When dust grains are very small (~ 10 nm) and accumulate only a few electron charges, the discrete nature of charge collection becomes important and a random-fluctuation charging model is more appropriate. In this case, the OML analysis presented here

is only qualitative. Additionally, since charging time scales with the inverse of the dust radius, the OML assumption that dust grains are in charge equilibrium might not be accurate. The OML-based calculation is nevertheless useful as it provides a sense of how the various currents affect dust charging and whether dust levitation is at all possible.

In terms of dust mobilization, these results show that initially the electrostatic force on the dust grain acts against dust motion: at the Moon's surface, the dust is negatively charged, the electric field is positive and the electrostatic force and gravity point towards the surface. This suggests that under these conditions, dust would not be mobilized. In general, however, dust could be mobilized by meteoroid bombardments and recent work by [15] and by [16] has shown that detachment/lofting of dust can be caused by dust-dust repulsion, instead of the interaction of a single charged dust grain with the sheath electric field. In any case, if the dust is mobilized, there is a range of altitudes ($\sim$1-12 m in this example) where the dust is positively charged, the electric field points away from the surface and, thus, the resulting electrostatic force points away from the surface. These are the conditions where dust can levitate through the balance between gravity and the electrostatic force [19, 9]. Figure 8 shows the electrostatic force (labeled as F_{el}) calculated on a spherical dust particle of radius 0.08 μm. A 0.08 μm particle was chosen as a representative size of a particle where stable levitation equilibria exist. Note that in this case the dust charge is $Q_d/e > 40$ (e is the positive elementary charge) already at an altitude > 1.4 m and asymptotes to $Q_d/e \sim 210$ away from the surface, justifying the use of the OML charging theory for this calculation. The electrostatic force points away from the surface when its value is positive. The figure also shows the absolute value of gravity (F_g), since gravity points towards the surface. For these parameters, there are two intersection points where gravity and the electrostatic force balance, i.e. there are two equilibrium points where dust can levitate. Analysis shows that the equilibrium point closer to the surface is unstable [7, 8], while the equilibrium point further away from the surface is stable. For the parameters considered, the stable levitation point occurs at about 5 m altitude.

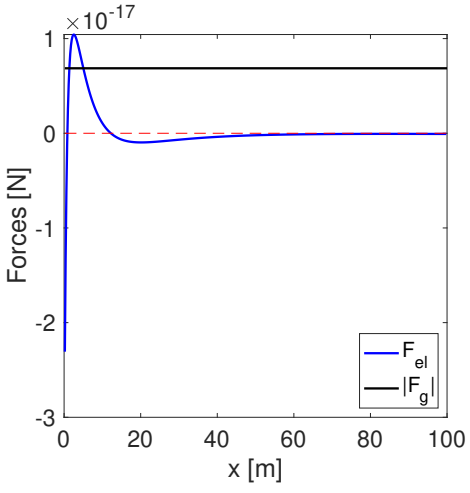

Figure 8: Gravitational force (black line) and electrostatic force (blue line) on a dust grain with radius 0.08 μm as a function of altitude. Red dashed line is reference for zero force.

As noted above, Schwan et al. [14] have argued that electrostatically lofted dust grains are not positively charged, but instead are negatively charged as a result of photoelectrons being trapped in the interstices between a clump of dust grains. Schwan et al. [14] also suggested that lofting might occur from the mutual repulsion of the negatively charged grains. Once a grain is detached from the surface, its charging is controlled by its interaction with the local plasma environment. Depending on the particle's initial launching velocity and charge, it may switch polarity prior to reimpact [20].

3.2. Motivation and Science Objectives

Beyond the effects of the dust charge on the lofting of the dust and its transport over potentially large distances, the charge state will also be important for future robotic/human exploratory missions. The sticking of particles (adhesion) to surfaces can be strongly altered by the charging of surfaces and the dust grains. The typical adhesion is influenced by both Van der Waals interactions and the dust/surface charge Coulomb interaction. Additionally, the presence of the spacecraft will modify the local plasma environment by creating shadows as well as emitting photoelectrons, both of which will modify the charging of

nearby regolith. To understand the dust contamination of spacecraft and to mitigate the effects of dust, it is thus of fundamental importance to quantify the charging state of the surface lunar regolith.

There are multiple ways to determine the charge of dust particles and their mass. Unfortunately, in most cases, a measurement only gives the charge-to-mass ratio. To separate charge and mass, it is necessary to conduct two measurements; one related to the dust dynamics (deflection, velocity, or energy measurement) and one directly due to the charge state via an electrical measurement (for example, measuring the mirror charge in a conductor). We identified three potential techniques for measuring the dust charge:

1. Measure the induced currents in a wire grid when particles fly by. This technique is established and has already been used in space experiments [39] (e.g., the Electrostatic Lunar Dust Analyzer (ELDA) experiment). Additionally, a similar sensor will also be flown on the Russian Luna-25 mission [40]. However, it has not yet been employed at an accuracy that would resolve the charge state down to low electron numbers (e.g., 10-100 electrons) as expected for dust particles in the sub-micrometer range.
2. Directly measure the dust particle charge or a mirror charge when a particle hits a surface and charges a small capacitor such as a pixel in an IonCCD. According to the detailed characterization of a line IonCCD detector used in the instrument IDS-2030 from OI Analytical [41], due to the small size and thus small capacitance in a CCD pixel, this technique can reach at least a similar if not significantly better sensitivity than did the one used in the ELDA experiment. It should be noted that the detector has been tested only for electrons, ions and molecules, not yet for charged dust particles.
3. Measure the surface potential of a test target that has dust particles on its surface. As surface potential and charge state of a particle are connected via the particle capacitance, knowledge of the particle surface potential can be used to determine its charge state. This technique [42] is in gen-

eral well established. However, it is not suitable for low number density particle coverings as the spatial resolution of the surface potential imaging is of the order of mm^2 or larger. As the surface charge is averaged with the particle charge, the measured average potential will be small or possibly undetectable for a low dust charging state and low number density of dust grains on the surface. Due to this inability to measure weak dust charges, we will not further analyze this approach. Nonetheless, this technique might have a significant value for characterizing the charge state in dedicated adhesion investigations where individual particles are placed on a coupon in a centrifuge to detect the critical force of detachment under the boundary conditions of different particle and surface materials. This technology could potentially be integrated in a device like that described in Section 4.

In the following section we discuss the methods and requirements for Techniques 1 and 2. Technique 2 could potentially also be used as a charge diagnostic for coupon-based measurements (see Section 4) where an IonCCD replaces a coupon target. It has to be noted that the currently available ionCCD sensor is a line CCD (1.5mm width, 24um x 2126 pixel height). To use this measurement technique effectively, it would be necessary to advance the sensor to a 2D planar detector of a suitable surface area (of order of cm^2).

3.3. Overall Design and Concept of Operations

We discuss here two kinds of experiments that have undergone partial (Technique 2) or detailed (Technique 1) developments for a very similar scenario to that considered here. Thus, these techniques can be applied with minor (Technique 1) or more substantial (Technique 2) adaptations to our goals.

3.3.1. Technique 1: The Electrostatic Lunar Dust Analyzer (ELDA) concept, reduced in size

The Electrostatic Lunar Dust Analyzer (ELDA) is a mature dust charge measurement technique [39]. When a dust particle enters the instrument, it

passes through a wire grid where each wire is connected to a charge sensitive amplifier. The mirror current signals received in the different wires can be used to reconstruct the particle trajectory and also calculate its charge. In the middle part of the instrument, the dust particle is subject to a strong electric field that modifies its path. This deflection is sensitive to the charge to mass ratio of the particle. The particle then flies through a second wire grid and the new particle velocity vector is measured and thus the extent of the deflection is measured. Knowing both the charge and the charge to mass ratio allows the derivation of both particle charge and mass separately.

The disadvantage of ELDA is its size (400x400x200mm) [39]. A down-scaled experiment setup (called the Electrostatic Dust Analyzer, EDA) as proposed in [43, 44] would fulfill the requirement for the dust charge and mass measurement, if the expected dust charging is beyond $1000e^-$ per particle. The sensitivity of this proposed experiment is given in the cited publications. The ELDA experiment is characterized [39] to have a noise floor of several hundred electrons and thus it would be suitable for charged particles with more than a few thousand electrons. The down-scaled EDA experiment can be expected to be a little more sensitive as the measured voltage scales with the inverse of the input capacitance. Still, the measuring of particles with a charge state below $1000e^-$ seems difficult with this method because of the high noise floor. To get a much better noise floor and sensitivity to detect particles with just a few electron charges, the sensor capacitance has to be significantly decreased and the connector length to the amplifiers reduced, as seen in Technique 2, and/or new, better trans-impedance/charge sensitive amplifiers need to be developed (as in [45, 46]) and adapted to this measurement technique.

The ELDA concept, even reduced in size, is operationally challenging for this specific science goal. Specifically, in addition to measuring the charge of mobilize dust particles, we also seek to quantify the charge of the undisturbed regolith particles on the lunar surface. Key to the ELDA measurement concept is that particles must travel through the instrument. While this is possible when the instrument is hosted by orbiters, measurement of the charge of regolith par-

ticles on the lunar surface would require those particles to be poured or dropped through the instrument, unless previously electrostatically lofted/levitated. Unfortunately, the very process of scooping and pouring particles will cause them to rub against neighboring particles, thus changing their charge through triboelectric charge exchange. Thus, the ELDA concept could be used to measure the properties of lofted grains, but not undisturbed surface grains.

3.3.2. Technique 2: Measuring the dust particle charge by charge transfer or mirror charge evaluation with an ionCCD detector

As mentioned in the description above for the ELDA/EDA experiment, the sensitivity of the direct charge measurement is related to the sensor (wire/pixel) capacitance. Smaller capacitance results in a larger signal, enabling the detection of low charge quantities. An example of this principle is used in photon detection using charge coupled devices (CCDs). Nowadays, CCDs with their small pixel size reach quantum efficiencies of about 50%. Thus every other photon is detected. The noise floor of such a detector can be just a few electrons per pixel, especially when the detector is cooled. It has to be noted that the noise floor is a floor current, thus the noise signal (voltage or number of noise electrons) also depends on the exposure time.

A standard CCD cannot be used for the proposed measurement. In a CCD, the incoming photon is transferred in a photo diode into an electrical signal (i.e., some free electrons). These electrons are accumulated in a capacitor associated with each pixel. After the exposure, each pixel is read out by shifting the accumulated charges in the individual pixel capacitors through the electrical chip infrastructure to be finally read out via an amplifier and digitizing circuitry. As might have become obvious, if the photon to electron layer in a standard CCD design can be removed and the incoming charges are directly collected by an exposed pixel capacitor, the rest of the CCD could perform as an electron, ion or even charged dust detector. This principle was realized several years ago by OI-Analytical. Their product is the ionCCD, where the chip pixel capacitors are exposed. The line ionCCD consists of 2126 pixels of 24μm $\times$ 1.5mm and a

detector area of around 76 mm^2.

[41] describes in detail the performance of an ionCCD sensor. In their experiments, the authors exposed the ionCCD to either an electron, an ion or a charged molecular beam within a vacuum environment. The measured standard deviation of multiple measurements from a given ion beam was determined to be about 300 electron charges for individual (non-averaged) CCD readout times of 15ms at room temperature conditions. This is the value that is interesting for individual counting events such as might appear if the detector was used as a dust charge detector. If the sensor is cooled, the noise floor can be expected to be significantly reduced and thus the sensitivity enhanced. An investigation of dust charge detection should be performed to identify the real sensitivity for this measurement scenario. Also it should be evaluated whether or not the effective sensor area can be significantly increased. To reach a similar order of detector cross-section as in ELDA/EDA, the sensor size must be increased by a factor of 100 while changing from a linear array sensor to a 2D sensor. Similar to the competition between optical CCD and CMOS sensors, a CMOS ionCCD approach might be also possible.

The ionCCD sensor requires dust particles to be deposited on the sensor in order to detect their charge. Additionally, since dust particles are not conductive, the ionCCD sensor would only measure the charge on the surface of the particle that makes contact with the sensor, reducing the charge sensed from the net charge on the particle. If an active method of depositing grains on the sensor is chosen (e.g. a scoop), then the charge measurement will be influenced by triboelectric charge exchange that occurs during this process, as in the ELDA instrument. Another option is to rely on electrostatic lofting (i.e. the natural transport of grains across the surface) to deposit particles on the sensor. This passive approach is risky, as the flux of lofted particles remains very uncertain. Additionally, there is a selection bias, as only particles that are sufficiently charged to be lofted and deposited on the sensor (as opposed to some other location) will be detected by the sensor. In order to measure the charge of lofted particles, it would be beneficial to expose the ionCCD at

different altitudes.

Both experiments described can be operated independently. While Technique 1 will lead to the particle charge as well as the particle mass, experiments using an ionCCD will only measure the particle charge but potentially with a better accuracy. Using both experiments together, where the ionCCD detector is placed at the outlet of the ELDA/EDA experiment, might combine the advantages of both detectors. A modified technique using the ELDA/EDA type detector to first determine the particle charge and mass and subsequently electrostatically stopping the particle and confining it in the instrument (active capturing) to perform detailed investigation on each trapped particle should also be considered. Concerning operational constraints, both types of experiment can be assumed to require the same operational support. The electronics should be temperature controlled, operating as close as possible towards the lower operational temperature limit as this will reduce noise in the system.

3.4. Size, Mass and Power Requirements

Both techniques can be expected to have similar electrical requirements while the volumetric needs of the ionCCD detector system (even with an enlarged CCD) are likely to be significantly smaller. In the following table, estimates for the EDA, the ionCCD as well as a combined instrument are given. Naturally, there would be increased mass, power and volume requirements if the instruments are mounted on a moveable platform.

3.5. TRL

The EDA system [43] is, to our knowledge, at a TRL level of approximately 4, mainly inherited from the ELDA developments. The underlying ELDA experiment was extensively tested as a breadboard system in the laboratory (TRL 4). The shrinking of the setup should be a straightforward operation. The ionCCD system seems to be at a TRL 2-3. The charge measurement capability has been demonstrated (not, however, for dust particles). Also, an areal (enlarged) sensor to be used as a dust detector has not yet been developed, to the best of our knowledge.

Table 3: Mass and power requirements for a dust charge measurement system. *We assume that the the amplifiers in the instrument only need to be powered, if the top layer detector grid detects an incoming particle. Thus, while waiting for events, most of the detector can remain in sleep mode. **The CCD detector naturally only consumes substantial power when it is read out. While it is collecting charges (dust particles), the power consumption is small.

	Volume (L)	Mass (g)	Power (W, peak)	Power (W, Continuous)
Technique 1 (EDA)	2	1000	< 10 W	< 5 W *
Technique 2 (enlarged ionCCD)	0.3	800	< 10 W	< 3 W **
Techniques 1 & 2 (EDA & enlarged ionCCD)	2.3	1500	< 15 W	< 8 W

3.5.1. Suggested areas of technology advancement

The ionCCD is currently only a line CCD with an effective surface area of around 76 mm^2. To be comparable in cross section to the EDA experiment and efficiently added to the EDA system as a combined experiment, the effective exposed CCD area must be increased by a factor of 100. Further the sensitivity can be improved by choosing different analog to digital (AD) conversion techniques/resolutions and cooling the chip. In the present form, the ionCCD is of limited use due to its small size, but after improvement it has a high potential to produce higher sensitivity charge measurements than does the EDA. Additionally, if the detector is expected to be exposed to excess dust (e.g. if dust is dropped into the device using a robotic arm), a method of cleaning the detector must be developed and evaluated.

While the EDA experiment has significant prior development, most current results have a charge resolution of approximately 1000 electrons, which is 1-2 orders of magnitude larger than some of the theoretical dust charging predictions. The EDA experiment could be advanced by using recently developed charge sensitive amplifiers that claim a noise floor of around 150 electrons rms [45] or even a few electrons (10e) [46].

4. Measuring Surficial Lunar Dust Transport with a Coupon-Camera System

4.1. Science Objectives

The main objective of this payload is the confirmation of the transport of dust particles in the lunar environment, especially due to electrostatic lofting. Additionally, the proposed payload provides an ideal instrument to assess how effectively dust can be removed from different surfaces using various remediation technologies [21]. Measurements of dust transport on the Moon are very limited, but recent analysis of the measurements of an Apollo 17 dust detector suggest that a transport rate of up to 100 μg cm^{-2} year^{-1} is possible [47]. This rate is then used as a constraint to define the criteria for measurements of active and passive dust transport. Here, "passive transport" will be used to refer to the motion of dust particles in the unperturbed lunar environment. "Active transport" will be used to refer to the motion of dust particles that is deliberately induced by agitation of the lunar soil. In both studies, we seek to measure the rate of deposition of dust onto targets and determine if there is a directionality to the flux.

4.2. Overall Design and Concept of Operations

To confirm the transport of dust particles in the lunar environment, we suggest an experiment where surfaces of different materials will be exposed to the unperturbed environment for a prolonged time. The surfaces will be monitored using a visual imaging system that resolves mm-sized patterns but not individual grains (which are likely micron-sized).

The Dust Collector Coupon (DCC) experiment will consist of three main components: two dust detectors that will be placed on the lunar surface and a camera. The dust detectors should be deployed at least one Debye length ($\sim$ 1 m) away from the main body of the lander because landed spacecraft will influence the local plasma environment. Note that the Debye length depends on the plasma density, which in turn depends on the illumination, which will

be influenced by the presence of the spacecraft, and solar wind conditions. The camera will be on a movable arm that can be positioned above the detectors with the ability to swing from one dust detector to the other.

Ideally, the camera and dust detectors should also translate vertically, allowing an investigation of the altitude variation of dust flux on spacecraft and the dust-loading of the lunar exosphere. It is likely that 'dust hopping' (short, nearly ballistic trajectories) are more common than long distance transport, and exposure of coupons at different altitudes would enable confirmation of this hypothesis. Additionally, any mobilization of dust caused by attraction of the particles to the dust detectors (e.g., caused by an electric potential difference or shadowing) will be reduced when the detectors are raised above the surface.

While the measurement of the net dust deposition rate will provide valuable information, we are particularly interested in understanding the flux of dust due to different processes. It should be relatively simple to identify dust flux due to exploration activities, as any mission would have knowledge of landing or roving activities taking place nearby. There are likely two main dust mobilization processes in the undisturbed environment: electrostatic dust lofting and micrometeoroid bombardment. In order to differentiate the contribution of these two processes, we suggest taking measurements of the dust deposition during a known meteor shower. This record of the dust flux signal of the meteor shower will enable the identification of additional meteoroid events to be identified in the data and deconvolved with electrostatically motivated dust motion.

A conceptual design for the dust detectors is illustrated in Figure 9. Here, a 8-cm diameter circular sample holder disk will have 8 to 12 sample coupons that will be 1.5 cm diameter (8) or 1 cm diameter (12). Nominally, three different materials will be evaluated for their efficacy of dust adhesion and removal. The baseline material (likely glass) will be placed in the four cardinal direction coupon holders. By using the same material for four coupons arranged at the cardinal directions, it will be possible to investigate the dependence of dust deposition on location, since coupons may experience different lighting conditions. The dust deposition may be influenced by the local solar illumination condi-

tions, the direction of travel of shadows on across the surface, and perturbation of the plasma environment by the spacecraft (although this effect will be minimized if the instrument is deployed on a sufficiently long boom). Two other materials (possibly spacesuit, solar panel or multi-layer insulation (MLI) samples) will be placed in the four remaining coupon holders (arranged diagonally to one another). The 1-1.5 cm coupon sizes were chosen to ensure that at least 100 dust grains of the mean lunar dust particle size (40 microns [48], [49]) would be collected in one month (see Table 4 and discussion below).

The sample holder disk will be placed on top of a rotary motor. All samples will be exposed continuously to the local plasma environment, and the motor would rotate the samples into the field of view of the camera for imaging.

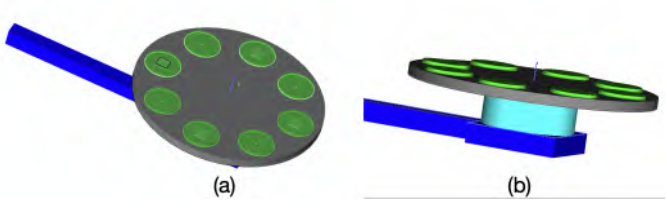

Figure 9: Two views of a sample holder disk. (a) Top view. The green disks are the individual sample coupons. The rectangular square in the disks represents an LED placed below four of the coupons. (b) Side view with the light blue cylinder indicating the placement of a motor for rotating the assembly. The individual sample coupons would be between 1 cm and 1.5 cm in diameter. The full assembly would be 8 cm in diameter.

Dust Detector A (DDA) will be used to monitor the background dust transport and will be the passive experiment. DDA will be placed as close to the surface as possible given the boom design (note: the boom is necessary to ensure that the instrument is at least 1 m from the spacecraft). Half of the DDA holders will also include an embedded LED below the surface to enable backlighting of the surface in order to make it easier to detect the dust particles that are collected on the surface. Using the previously reported transport rate of lunar dust, it is possible to estimate the rate of dust coverage of the sample coupons. Assuming dust particles have an average mass density of 1.5 g/cm^3

and sizes ranging from 1 to 40 micron diameter, and that the DDA is exposed to the lunar environment for 1 month, Table 4 presents calculations of the number of dust grains and the fractional dust coverage of the coupons. Higher grain density would decrease the number of grains on a coupon, thus resulting in less coverage of the coupon.

Table 4: Dust transport and collection in 1 month assuming grains of a single size and a flux of 100 μg cm^{-}2 yr^{-}1 [47].

		1 cm coupon	1.5 cm coupon	
Diameter (micron)	Mass (g)	Particles	Particles	Coverage (percent)
1.0	7.85×10^{-13}	8.3×10^{6}	1.9×10^{7}	8.3
2.0	6.28×10^{-12}	1.0×10^{6}	2.3×10^{6}	4.2
5.0	9.82×10^{-11}	6.7×10^{4}	1.5×10^{5}	1.7
10.0	7.85×10^{-10}	8.3×10^{3}	1.9×10^{4}	0.8
20.0	6.28×10^{-9}	1.0×10^{3}	2.3×10^{2}	0.4
40.0	5.02×10^{-8}	1.3×10^{2}	2.9×10^{2}	0.2

Based upon these calculations, photographs of each coupon will be taken at one week intervals. Consequently, DDA will generally have a low data rate. We would propose a minimum of a 3 month duration to make these measurements.

Dust Detector B (DDB) will be placed near an instrument that can perturb the local lunar surface and lead to the possible lofting of dust particles. If lofting occurs, it will load a substantial population of dust grains onto the detector and so enable mitigation studies. Alternatively, DDB could be used in coordination with the dust loading device discussed in Hirabayashi et al. [21]. DDB will be used primarily to study dust removal from different materials. While the design of DDB is similar to DDA, there are several important differences. The sample coupons on DDB will likely consist of non-transparent materials (e.g., samples based on spacesuit material, spacecraft body materials, etc.), so the embedded LEDs of DDA will not be required. DDB will also have the ability to apply

an electrostatic bias voltage to the coupons to either enhance the collection of dust grains or aid in electrostatic repulsion experiments. Note that a separate dust sample carousel is required for DDB because any method of active dust loading would contaminate measurements of the background, undisturbed dust environment that will be probed with DDA.

DDB would be imaged using the same camera as DDA. Depending upon which experiment is being performed, images would be recorded at 50 frames/sec for short bursts of up to 30 seconds to capture the time evolution of dust deposition during active experiments. To limit the data downlink volume, it may be desirable to do some image processing on-board the lander. For example, it may only be possible to send down the first, last and a few intermediate images at full grayscale. In this case, the additional high framerate images could be downlinked after threshholding and binarizing on the lander.

DDB will also evaluate a variety of dust mitigation/removal approaches. The goal of these experiments will be to both gain insights into the forces that allow the dust to adhere to surfaces and to understand how a combination of mechanical and electrical based approaches may be used to remove the dust particles. If a dust removal technology is also integrated into DDA, then the coupons could be cleared and the experiment repeated at multiple altitudes, thereby investigating dust flux as a function of altitude.

We note that there are a series of possible descope options for this instrument. Firstly, while we propose to have two sample disks, it would also be possible to fly a single sample disk. In that case, we would prioritize the passive experiment, to study the natural dust deposition. The camera set-up could be mobile or fixed. The benefit of the mobile camera (even for a single sample disk) is that the camera could be moved away from the sample during the collection phase, to eliminate the camera's perturbation of the local plasma environment.

An additional descope option would be to eliminate the vertical translation of the dust detector(s) and camera. This would simplify the operations and decrease the weight of the arm (eliminating the need for a horizontal track and motor). If fixed, the preferred fixed altitude of the experiment would be as close

as possible to the lunar surface, as it is likely that the majority of electrostatic dust lofting occurs in short hops, rather than large scale, high altitude transport. An alternate design would be to include multiple stationary dust collectors at varying altitudes. This design would eliminate the need for a vertical translation mechanism, but would likely have increased mass and volume requirements.

It is important to note that the utility of this instrument is increased when a dust removal technology (as discussed in Hirabayashi et al. [21]) is integrated into the design. Firstly, coupons observed by cameras are a natural method to measure the efficacy of removal technologies. Secondly, removing dust from coupons (i.e. 'refreshing' the coupons) would enable more sensitive measurements (since there would be less risk that the camera would fail to observe differences in dust coverage between two images of a given coupon) as well as enable the experiment to be reinitialized for different experimental conditions (e.g., altitude, time of day).

Both DDA and DDB will be based on rotary stages. A rotation slow enough to avoid disturbances (< 0.1 revolutions/sec) will move each sample coupon into the field of view of the camera in order to image the collected dust particles. However, a much faster rotation (up to 10 revolutions/sec) may be effective at removing dust from the surface - serving as a built-in dust removal technology that would not require additional parts. Additionally, by performing a series of staged experiments at different rotation speeds and imaging the remaining dust grains, it will be possible to estimate the strength of the adhesive forces.

4.2.1. Camera

The proposed camera builds on a legacy of spacecraft camera systems that have been developed over several decades. In particular, the base design used for two instruments on board the recent Rosetta mission is particularly well-suited. Both the COSISCOPE, part of the COmetary Secondary Ion Mass Analyser (COSIMA) instrument on board the orbiter, and the Comet Infrared and Visible Analyser (ÇIVA), on board the lander (Philae), used a miniature camera system developed by the IAS group in Orsay, France [50, 51]. The

COSISCOPE was integrated within the COSIMA instrument and was used to study dust samples collected on gold coupons. It had a total mass of 460 g including the mechanical structure and optical elements. It could image an area of 14×14 mm^2 with a magnifying power of 1, resulting in a spatial resolution of about 14 micron. It was designed to image individual particles on coupons made of gold and silver blacks and was therefore equipped with two low-incidence, red LEDs (positioned at 5 and 10 deg, respectively). Its mean power was 4 W. The lander instrument, ÇIVA consisted of multiple miniature panoramic cameras (CIVA-P; f/10; resolution 1 mm - meters), an optical microscope (CIVA-M/V; f/20 for a diameter of 3 mm; resolution 7 μm - 1mm), and a scanning IR microscope (CIVA-M/I). The microscope had a mass of 276 g, measured $70 \times 50 \times 94$ mm, and had a power consumption 2.2 W and three colored LEDs were used to illuminate the surface of 67P (525 nm, 640 nm, 880 nm).

The base camera will be mounted at the end of a movable arm that can extend over the dust detectors. The base camera will consist of a CCD/CMOS sensor that is integrated into a lens system. The camera will be facing downward (towards the lunar surface) and will be focused on the dust grains on DDA or DDB.

An ideal imaging system will have a field-of-view of 20 mm x 20 mm and spatial resolution of at least 15 microns/pixel. The separation between the camera and the dust detectors would be constrained by these two limits. The camera surface would also house a ring of visible and UV LEDs to illuminate the dust coupons from above as well as a source of UV for charging manipulation.

We propose that the camera have a 4 Mpixel sensor (2048 x 2048 pixels, twice the detector size of the Rosetta instruments) with a full resolution frame rate of 50 frames/sec. The camera should have the ability to use software to select a smaller region of interest (ROI) in order to achieve faster imaging speeds, if needed.

An optional capability of the camera would be to add one or two additional "side views" to the camera assembly. These would be equipped with lenses that would provide near (1 – 5 m) and distant (e.g., to the horizon) views

of the environment around the lander. This upgraded capability would allow additional measurements to be made of the lunar horizon glow phenomenon as well as enabling the possibility to look for naturally lofted and levitated dust particles. A conceptual drawing of the camera is shown in Figure 10.

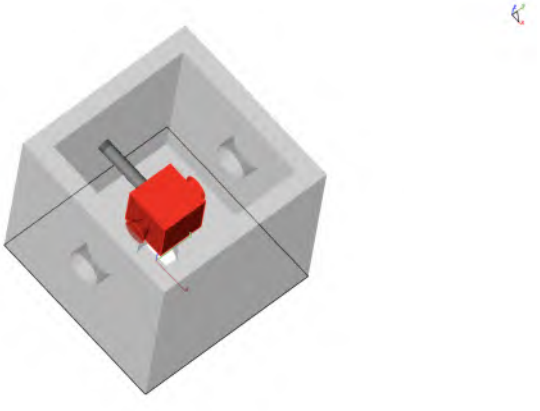

Figure 10: Conceptual drawing of the three-sensor camera head option. The base camera design will use a single camera sensor pointing downward toward the samples. With the optional three sensor design, it may be possible to adapt the side cameras for viewing dust levitation on the lunar horizon.

4.2.2. Operational Constraints

The DCC instrument will generally have a limited operational schedule, but would ideally operate for several months, given the expected slow rate of dust deposition. For the measurements of the unperturbed dust transport using dust detector A (DDA), each sample would be measured one or two times per week. Since measurements are simply high resolution photographs, this could be done as an automated process via pre-programmed scripts. Operation over multiple months would require the spacecraft electronics to revive after lunar night.

The measurements using dust detector B (DDB) will require more resources. If experiments are performed in conjunction with a dust perturbation experiment, then the camera would need to record video, perhaps up to several hun-

dred frames per second for up to 10 seconds in order to view the deposition of dust particles. Additionally, the motor for DDB would need to spin up to 10 rev/sec to remove the dust grains from the surface of the samples.

Additionally, we have also considered the use of the aforementioned UV source and electrostatic biasing to aid in dust removal. A bipolar bias voltage capable of delivering voltages in the range (+100 V to -100 V) would be the ideal instrument for this. Laboratory testing would need to be performed in order to determine the most effective UV-LED configuration for modifying the charge of the lunar dust particles.

4.3. Estimated System Requirements

The size, mass and power requirements for the system are estimated in Table 5.

Table 5: Estimated Mass and Power Requirements for dust accumulation carousel.

	Mass (g)	Power (W)
Camera Structure	1700	0
Camera + Lens assembly	400	4
Piezo-motor	300	20
Sample Holder Disk + LEDs	50	0
Samples (8)	5	0
Fold-out Deployment Arm (optional)	TBD	6
Deployment Arm with Vertical Translation (optional)	TBD	TBD

Table 6 gives a discussion of the estimated TRL of the components of this experiment. While the deployment mechanism and vertical translation stage are listed as low TRL, it is likely that these mechanisms would draw on prior designs. Future work should be done to identify and mature piezo-motors capable of spinning the sample disk in the lunar surface thermal environment.

Table 6: TRL estimates for Dust Collection Coupon components

	TRL	Comment
Camera Structure	6	Used on previous missions, but may require customization
Camera+Lens assembly	6	Used on previous missions, but may require customization
Piezo-motor	3	Lab testing needed
Carousel	4	Lab testing needed
Samples (8)	4	Lab testing needed
Fold-out Deployment Arm (optional)	4-5	Draw from Heritage
Deployment Arm with Vertical Translation (optional)	4-5	Draw from Heritage

5. Dedicated Lunar Horizon Glow Measurements

5.1. Science objectives

The primary objective of the proposed payload is to observe dust levitation at/over the lunar horizon. Levitating dust is likely to be easiest to observe as lunar horizon glow, which is hypothesized to be caused by light forward-scattering off of dust particles above the lunar surface. Recent reanalysis of Apollo imagery questions whether prior observations of lunar horizon glow were produced instead by zodiacal light [4]. Conclusively observing and characterizing the structure of a lunar horizon glow would provide strong constraints on the existence of levitating dust. We now summarize the existing horizon glow observations.

The crew of Apollo 17 observed the horizon glow [52] from near surface to an altitude of a few hundred km at the terminator (the Apollo orbiter altitude was 100 km – 120 km). Their analysis showed that number densities of 0.1 μm particles may be 10^{-1} cm^{-3} at 1 km, 10^{-2} cm^{-3} at 10 km, and $10^{-5} - 10^{-6}$ cm^{-3} at $100 - 200$ km.

Surveyor 5, 6, and 7 observed a horizon glow along the western lunar horizon one hour after local sunset [53, 1]. The observation was interpreted as a cloud of dust grains 3 to 30 cm above the local horizon with a column density of 5 grains/cm^3 located near the local horizon which was 200 m west of the Surveyor 7 spacecraft. The glow was observed within 3 degrees on either side of the sunset line to decrease in brightness following sunset. The horizon glow region is approximately 10 – 30 cm both in vertical extent and in depth along the television line-of-sight [1].

Rennilson and Criswell [1] state that the maximum luminance of the horizon glow observed by the Surveyor missions was ~ 0.3 cd/cm^2. Any imager should have a full range of wavelengths, as well, to match the observations of the Surveyor TV camera. Exposure times should be controllable from ms to s. It is expected that the imaging campaign would be focused on the dawn or dusk period and that a large number of images with varying exposures would be taken during this period. If there is limited downlink bandwidth, it may be possible to identify images with anomalous brightening (i.e. evidence of horizon glow) via on-board processing.

Although high altitude dust levitation has also been hypothesized [54], no evidence for electrostatically-driven km-altitude dust was observed by the LADEE mission's LDEx dust detector [5].

Subsequent numerical models have studied the oscillatory behavior of levitating dust, predicting the size of particles that could levitate and the altitude at which levitation should occur (e.g., [7, 8]). These studies predict that dust with particle sizes < 100 nm could levitate at an altitude of ~ 10 m [8]. Additionally, dust levitation is strongly dependent on the surface topography, which controls the surrounding electric field [55].

5.2. Characteristics of Heritage Instrument

Based on the observation conditions of the Surveyor 7 slow-scan TV camera, we recommend the Optical Navigation Camera Telescope (ONC-T) on-board the Hayabusa2 spacecraft [56, 57, 58, 59] and the Particle Size Spectrometer (LCPS)

flown on the Pioneer Venus Sounder Probe [60] as prototype instruments to observe the Lunar Horizon Glow.

ONC-T is part of a camera suite that also includes two wide-angle cameras and assorted electronics packages. ONC-T is a telescopic CCD camera [57] with specifications as shown in Table 7. Given these capabilities, a 2 km $\times$ 2 km area at 20 km range is observable, and so is a 10 m $\times$ 10 m area at 100 m range. Although the mass and power are not publicly available, we assume a camera system mass less than 5 kg and a power consumption less than 10 W during maximum usage. The camera TRL is 9.

The ONC-T's exposure time can be controlled between 5.44 ms to 200 sec. It can also be set at 0 sec for 'smear data' [57] to enable the calibration and removal of camera dark current noise. ONC-T is also equipped with a filter wheel system having seven band-pass filters and one panchromatic glass window. The band-pass filters required to observe levitating dust may differ from those used on Hayabusa2 and may depend on the region of deployment (due to chemical differences in the regolith).

LCPS measures the particle sizes between 0.5 and 500 μm using shadowgraph and light scattering techniques [60]. It can also measure the aspect ratio of particles larger than 50 μm in size. Combining multiple measurements, the vertical variation of particle concentration (using 34 particle size bins) can be reconstructed. The required power of this probe is 20 W, and the mass is 9.5 lbs (4.3 kg). Because it was flown with the Pioneer Venus Sounder Probe, its TRL is 9.

5.3. Operational Constraints

As the observational conditions (locations, time, mission period, robotic or human missions, etc.) still need to be determined, we assume that the strawman instruments above will be autonomously deployable. The camera should point to the lunar horizon and observing conditions may be improved after sunset (when forward scattering off the grains would be observable). Thus, the ability for the camera to withstand low temperatures is preferred. The height of the

Table 7: Characteristics of the ONC-T camera flown on the Hayabusa2 spacecraft. Values from Kameda et al. [57].

Specification	Values
Effective lens aperture	15.1 mm
Field of view	6.27°× 6.27° (Optical black pixels are excluded)
CCD format	1,056 pixel × 1,024 pixel
CCD pixel size	13 μm
Pixel resolution	22.14 arcsec
A/D conversion	12-bit

camera may have to be adjusted to account for local topography; however, the extent of adjustment may be constrained by the lander's capability. The imager must be mounted on a stable platform in order to facilitate long exposure times. Additionally, a wide range of exposure times ranging from ms to hour(s) may be necessary to observe levitating dust, depending on the light condition. Thus, the selected imager should support this large variation in exposure times.

5.4. Areas Requiring Additional Analysis or Development

There are several areas of scientific or technical development necessary to increase the science return of a camera dedicated to observing horizon glow.

Improved models of the predicted dust density to be observed should be developed in order to support the selection of optics for this task. Additionally, light scattering by levitating dust particles may be affected by the background noise such as zodiacal light and constantly existing dust clouds. It is necessary to establish methodologies for disambiguating horizon glow from such background scattering [4, 61].

Depending on how long the cameras are placed in the shadowed region, they will need proper protection to conduct the required observations in the expected thermal environment. The timing of observations needs to be determined. Technology development is required to keep the cameras operational in the shadowed regions.

The cameras may be exposed to dust particles if located outside a lander or lunar habitat. Accumulated dust on optics may obscure or degrade camera performance. Thus, methods to remove accumulated dust or prevent accumulation are necessary. One possible solution for the lens may be to insert sacrificial surfaces (consisting of thin, clear, polymer layers) directly on the lens surface to protect it from dust particles and then remove these when necessary.

Dust levitation is likely to be controlled by the physical properties of particles (shapes, size, and mineral compositions). Adding additional filters to constrain these properties is one way to address this issue. Future investigations are needed to identify the proper wavelengths to characterize the physical properties of levitating dust particles.

Because of increased computational capability, it is possible to collect video observations of the horizon. The time-evolution of the horizon glow is part of the critical information of its characteristics. Future investigation should analyze the necessity of collecting both still picture and video data. If video observations are required, the frame rate and duration of monitoring should be determined.

The horizon glow's structure (location, shape, height, and distribution) is key to understanding its formation and evolution mechanism. Stereophotogrammetry may improve understanding of the phenomenon and the feasibility of such observations should be investigated.

Surface features (e.g., craters and boulders) may change the baseline dust levitation environment. Thus, future investigations should identify morphological characteristics that are likely to promote dust levitation, which would be preferred deployment locations.

6. Discussion

While electrostatic dust motion on the lunar surface has been hypothesized for almost 50 years, there is no conclusive evidence that it occurs. However, the possibility of dust transport due to electrostatic forces has significant implications for our understanding of the evolution of the lunar surface as well as

the risks associated with spacecraft and astronauts on the lunar surface. Lunar dust may pose a threat to camera optics, thermal control systems, spacesuit materials, and bearings and seals. Furthermore, these studies may also provide important, new insights for dust transport on other airless bodies throughout the solar system. In the intervening years since the hypotheses of electrostatic lofting and levitation were first proposed, there have been significant advances in our models of the near-surface plasma environment and charging processes for surficial regolith particles. Additionally, there is now a wealth of experience to draw from in the design and operation of Langmuir probes and cameras in space and on planetary bodies. A series of relatively simple instruments on the lunar surface could provide crucial information to constrain the phenomena of electrostatic dust motion as well the potential risk to future exploration vehicles.

We have discussed four main instruments to characterize the lunar dust-plasma environment: a Langmuir probe to characterize the plasma environment, dust charge measurements, a coupon-camera system to measure the rate of dust transport, and dedicated Horizon Glow observations. Langmuir probes are used commonly in terrestrial labs and have flown on many spacecraft. Similarly, the cameras necessary for both the coupon system and the Horizon Glow observations could draw on the long history of cameras flown in space. The key technologies for these instruments are not novel, however, they must be customized for this specific science investigation. The dust charge measurement is a more challenging technology. Even in terrestrial labs, methods to measure charge on individual dust grains on a surface in a plasma *without changing the charge state* of the dust grains are lacking. Most technologies to measure charge on particles require dropping grains, either to induce a current in a grid of wires or into a Faraday cup. This requires the dust grains to either naturally fall into a device, which can be difficult to induce, or to be scooped and poured into the device, which results in modified charge states as the grains tribocharge during collisional processes. Entirely new charge measurement technologies that can operate above an undisturbed bed of regolith would advance this science.

Assuming that the proposed instruments are hosted on a single, stationary

lunar lander, science return would be enhanced if three of the instruments (the Langmuir probe, the dust collection coupons and the dust charge probe) were deployed on booms. In the case of the dust charge probe, the boom would be used to position the instrument in various locations about the lander, leading to measurements in different shadowing conditions (leading to different exposures to the solar wind) and possibly different regolith packing or chemical compositions. For the Langmuir probe and the dust collection coupons, vertical translation is perhaps more critical than lateral translation. Specifically, the electric field is the spatial derivative of the electric potential, thus it is necessary to measure plasma potential as a function of height in order to calculate the vertical electric field that can counteract gravity, leading to lofting and levitation. Additionally, we note that the dust accumulation coupons do not uniquely detect electrostatic levitation: accumulated dust could be released and transported by other mechanisms (e.g. ballistic transport following a micrometeoroid impact or exploration activity). While the rate of dust accumulation and its sensitivity to illumination and material properties is of interest to spacecraft designers, assessing the rate of dust accumulation as a function of height above the surface would give insight into the source and transport mechanism of the dust (in addition to its contribution to enabling exploration). Thus, lightweight, deployable booms capable of lateral and especially vertical translation are key to maximizing the science returns of these instruments.

The four instruments described here would each, individually, provide valuable data on the lunar dust-plasma environment. When hosted by a single lander, or on operated in missions flown in quick succession, these instruments provide the observational evidence of undisturbed phenomena as well as key modeling input parameters to revolutionize our understanding of near surface lunar dust-plasma interactions. Dedicated, modern instruments to observe lunar horizon glow and dust deposition rate will provide the first intentional measurements of electrostatic dust transport on the lunar surface. The Langmuir probe and dust charge instrument would provide measurements of the plasma and dust charging environments that are key for correctly modeling and predicting

electrostatic dust motion. When flown as an instrument suite, grain charge measurements and plasma environment measurements could be combined to predict electrostatic lofting and transport (what size particles are lofted and what are their trajectory characteristics?), and then those predictions compared to dust deposition observations. Models informed and validated in this way could be compared to horizon glow observations.

The payloads that we have identified here focus heavily on dust plasma interactions for the purpose of testing long-standing hypotheses concerning electrostatic dust motion on the Moon. There are several additional investigations that would improve models of electrostatic lofting and levitation on the Moon, and should be pursued in subsequent investigations. Note these investigations would require other instruments beyond those described in this paper. Several of these investigations are also relevant to other areas of lunar science. We list these objectives and describe their relevance to the electrostatic dust motion and other science and exploration objectives here:

1. *Measure cohesion/adhesion of regolith.* Cohesion and adhesion of lunar dust particles are strongly dependent on the physical properties of particles and local electrostatic forces. Prior work has demonstrated that cohesion significantly influences the feasibility of electrostatic lofting for small regolith particles [10]. Additionally, regolith cohesion influences soil properties that will drive exploration activities (e.g., rover traction and drilling efforts). Adhesion (the attraction of regolith to other materials) measurements are necessary to design dust remediation technologies.
2. *Evaluate whether electrostatically lofted/levitating dust poses a hazard to exploration vehicles.* Electrostatic dust transport is most likely to pose a hazard to exploration vehicles through dust accumulation. Thus, it is necessary to understand if the presence of surface exploration vehicles will promote electrostatic lofting and if detached particles will be attracted to exploration vehicles. While this science objective is informed by our dust accumulation coupon payload, there is additional work to be done

to evaluate specifically if and how exploration vehicles promote dust lofting/levitation.

3. *Characterize the effects of plume impingement on dust properties related to interactions with plasmas.* Prior work [62, 63] has shown that landing on the lunar surface alters the regolith in regions tens of meters in diameter about the landing site. In addition to the removal of small regolith particles, the charging and cohesive properties of the regolith may be changed by chemical contaminants. Any measurements made by a stationary, landed vehicle are likely to be influenced by the landing process. Understanding the effect of contamination on regolith-plasma interactions will influence our interpretation of other scientific observations, as well as influence the predictions of dust hazards to future surface exploration missions.

4. *Measure the triboelectric charging of lunar regolith.* The fundamental physics of triboelectric charging of dielectric particles remains poorly understood. Due to the lack of an atmosphere on the Moon, charge will not dissipate as readily as in terrestrial environments. Additionally, many exploration activities (roving, digging, walking [17]) will cause triboelectric charging. Tribocharging will influence the likelihood of electrostatic dust lofting, although it is unknown whether it will increase or decrease lofting frequency.

5. *Characterize the size and shape of lunar regolith particles.* The size and shape of lunar regolith have been measured in detail using Apollo samples. However, the sample locations and characterization of micron-scale particles are limited. All attempts to measure and model electrostatic phenomena in situ will require an understanding of the size and shape distributions of lunar regolith particles. Whether this characterization of the dust particles is performed in-situ or on returned samples, this data is necessary to properly interpret measurements of dust-plasma interactions.

7. Conclusions

Electrostatically-motivated dust motion (including lofting and levitation) on the Moon has been hypothesized and studied for the past 50 years. However, there have been no dedicated instruments to detect these phenomena in situ and no conclusive observational evidence. Electrostatic lofting and levitation are of interest to planetary scientists seeking to understand the evolution of the lunar surface as well as to spacecraft designers that seek to predict the hazard of lunar dust to planned exploration vehicles. We have identified four payloads to be deployed on a lunar lander that are based on relatively mature technology and would measure key parameters to improve our understanding of dust-plasma interactions near the lunar surface. A Langmuir probe, which have been flown on a variety of other space missions, would, for the first time, measure the plasma properties in the near-surface photoelectron sheath, providing a key input for modeling efforts. A charge measurement device would detect the charge of regolith particles, providing a key constraint for lofting and levitation models. We propose dust accumulation coupons, which would measure the rate of dust accumulation on surfaces as a function of material properties and illumination conditions. Finally, we propose a set of modern cameras to look for evidence of the Lunar Horizon Glow. The measurements made by this suite of instruments would also significantly improve our understanding of the feasibility and risk posed by electrostatic dust mobilization on the lunar surface.

8. Acknowledgement

This work was supported by the Biological and Physical Science Division of NASA's Science Mission Directorate and by the Game Changing Development Program of NASA's Space Technology Mission Directorate through a contract with the Jet Propulsion Laboratory, California Institute of Technology.

References

[1] J. J. Rennilson, D. R. Criswell, Surveyor observations of lunar horizon-glow, The Moon 10 (1974) 121–142.

[2] O. E. Berg, F. F. Richardson, H. Burton, Apollo 17 Preliminary Science Report, NASA, 1973.

[3] T. Murphy Jr, E. Adelberger, J. Battat, C. Hoyle, R. McMillan, E. Michelsen, R. Samad, C. Stubbs, H. Swanson, Long-term degradation of optical devices on the moon, Icarus 208 (2010) 31–35.

[4] D. A. Glenar, T. J. Stubbs, J. E. McCoy, R. R. Vondrak, A reanalysis of the Apollo light scattering observations, and implications for lunar exospheric dust, Planetary and Space Science 59 (2011) 1695–1707.

[5] M. Horányi, J. Szalay, S. Kempf, J. Schmidt, E. Grün, R. Srama, Z. Sternovsky, A permanent, asymmetric dust cloud around the moon, Nature 522 (2015) 324–326.

[6] J. Szalay, M. Horányi, The search for electrostatically lofted grains above the moon with the lunar dust experiment, Geophysical Research Letters 42 (2015) 5141–5146. doi:doi:10.1002/2015GL064324.

[7] A. Poppe, M. Horanyi, Simulations of the photoelectron sheath and dust levitation on the lunar surface, Journal of Geophysical Research: Space Physics 115 (2010) n/a–n/a. URL: http://doi.wiley.com/10.1029/2010JA015286. doi:doi:10.1029/2010JA015286.

[8] C. Hartzell, D. Scheeres, Dynamics of levitating dust particles near asteroids and the moon, Journal of Geophysical Research: Planets 118 (2013) 116–125.

[9] C. Hartzell, Dynamics of 2D electrostatic dust levitation at asteroids, Icarus 333 (2019) 234–242.

[10] C. Hartzell, X. Wang, D. Scheeres, M. Horányi, Experimental demonstration of the role of cohesion in electrostatic dust lofting, Geophysical Research Letters 40 (2013) 1038–1042.

[11] X. Wang, M. Horányi, S. Robertson, Experiments on dust transport in plasma to investigate the origin of the lunar horizon glow, Journal of Geophysical Research 114 (2009) A05103.

[12] A. Sickafoose, J. Colwell, M. Horanyi, S. Robertson, Experimental levitation of dust grains in a plasma sheath, Journal of Geophysical Research 107 (2002) 1408.

[13] J. Halekas, G. Delory, R. Lin, T. Stubbs, W. Farrell, Lunar Prospector observations of the electrostatic potential of the lunar surface and its response to incident currents, Journal of Geophysical Research 113 (2008) A09102.

[14] J. Schwan, X. Wang, H.-W. Hsu, E. Grun, M. Horányi, The charge state of electrostatically transported dust on regolith surfaces, Geophysical Research Letters 44 (2017) 2017GL072909.

[15] X. Wang, J. Schwan, H.-W. Hsu, E. Grun, M. Horányi, Dust charging and transport on airless planetary bodies, Geophysical Research Letters 43 (2016) 6103–6110.

[16] M. Zimmerman, W. Farrell, C. Hartzell, X. Wang, M. Horányi, D. Hurley, K. Hibbitts, Grain-scale supercharging and breakdown on airless regoliths, Journal of Geophysical Research: Planets 121 (2016) 2016JE005049.

[17] T. Jackson, W. Farrell, R. Killen, G. Delory, J. Halekas, T. Stubbs, Discharging of roving objects in the lunar polar regions, Journal of Spacecraft and Rockets 48 (2011) 700–703.

[18] C. Hartzell, D. Scheeres, The role of cohesive forces in particle launching on the moon and asteroids, Planetary and Space Sciences 59 (2011) 1758–1768.

[19] T. Nitter, O. Havnes, F. Melandsø, Levitation and dynamics of charged dust in the photoelectron sheath above surfaces in space, Journal of Geophysical Research 103 (1998) 6605–6620.

[20] C. Hartzell, M. Zimmerman, C. Hergenrother, An evaluation of electrostatic lofting and subsequent particle motion on bennu, Planetary Science Journal 3 (2022) ac5629.

[21] M. Hirabayashi, C. Hartzell, P. Bellan, D. Bodewits, G. Delzanno, T. Hyde, U. Konopka, E. T. Jr., H. Thomas, I. Hahn, U. Israelsson, Electrostatic dust remediation for future exploration of the moon, Acta Astronautica (Submitted).

[22] M. Y. Pustylnik, M. A. Fink, V. Nosenko, T. Antonova, T. Hagl, H. M. Thomas, A. V. Zobnin, A. M. Lipaev, A. D. Usachev, V. I. Molotkov, O. F. Petrov, V. E. Fortov, C. Rau, C. Deysenroth, S. Albrecht, M. Kretschmer, M. H. Thoma, G. E. Morfill, R. Seurig, A. Stettner, V. A. Alyamovskaya, A. Orr, E. Kufner, E. G. Lavrenko, G. I. Padalka, E. O. Serova, A. M. Samokutyayev, S. Christoforetti, Plasmakristall-4: New complex (dusty) plasma laboratory on board the international space station, Review of Scientific Instruments 87 (2016) 093505. URL: https://doi.org/10.1063/1.4962696. doi:doi:10.1063/1.4962696. arXiv:https://doi.org/10.1063/1.4962696.

[23] S. Popel, L. Zelenyi, A. Golub', A. Dubinskii, Lunar dust and dusty plasmas: Recent developments, advances, and unsolved problems, Planetary and Space Science 156 (2018) 71–84. URL: https://linkinghub.elsevier.com/retrieve/pii/S0032063317302325. doi:doi:10.1016/j.pss.2018.02.010.

[24] T. Stubbs, W. Farrell, J. Halekas, J. Burchill, M. Colier, M. Zimmerman, R. Vondrak, G. Delory, R. Pfaff, Dependence of lunar surface charging on solar wind plasma conditions and solar irradiation, Planetary and Space Science 90 (2014) 10–27.

[25] Z. Sternovsky, P. Chamberlin, M. Horányi, S. Robertson, X. Wang, Variability of the lunar photoelectron sheath and dust mobility due to solar activity, Journal of Geophysical Research 113 (2008) A10104. doi:doi:10.1029/2008JA013487.

[26] I. A. Kuznetsov, A. V. Zakharov, G. G. Dolnikov, A. N. Lyash, V. V. Afonin, S. I. Popel, I. A. Shashkova, N. D. Borisov, Lunar Dust: Properties and Investigation Techniques, Solar System Research 51 (2017) 611–622. URL: http://link.springer.com/10.1134/S0038094617070097. doi:doi:10.1134/S0038094617070097.

[27] H. M. Mott-Smith, I. Langmuir, The Theory of Collectors in Gaseous Discharges, Physical Review 28 (1926) 727–763. URL: https://link.aps.org/doi/10.1103/PhysRev.28.727. doi:doi:10.1103/PhysRev.28.727.

[28] J. Olson, N. Brenning, J.-E. Wahlund, H. Gunell, On the interpretation of Langmuir probe data inside a spacecraft sheath, Review of Scientific Instruments 81 (2010) 105106. URL: http://aip.scitation.org/doi/10.1063/1.3482155. doi:doi:10.1063/1.3482155.

[29] J. E. Allen, The plasma-sheath boundary: its history and Langmuir's definition of the sheath edge, Plasma Sources Science and Technology 18 (2008) 014004. URL: https://doi.org/10.1088/0963-0252/18/1/014004. doi:doi:10.1088/0963-0252/18/1/014004.

[30] P. Bellan, Fundamentals of Plasma Physics, Cambridge University Press, 2008, pp. 64–68.

[31] S. T. Lai, An improved Langmuir probe formula for modeling satellite interactions with near-geostationary environment, Journal of Geophysical Research 99 (1994) 459. URL: http://doi.wiley.com/10.1029/93JA02728. doi:doi:10.1029/93JA02728.

[32] E. C. Whipple, Potentials of surfaces in space, Reports on Progress in Physics 44 (1981) 1197–1250. URL: https://iopscience.iop.org/

article/10.1088/0034-4885/44/11/002. doi:doi:10.1088/0034-4885/44/11/002.

[33] S. Bose, M. Kaur, P. K. Chattopadhyay, J. Ghosh, Y. C. Saxena, R. Pal, Langmuir probe in collisionless and collisional plasma including dusty plasma, Journal of Plasma Physics 83 (2017) 615830201.

[34] J. E. Allen, Probe theory - the orbital motion approach, Physica Scripta 45 (1992) 497–503. URL: https://iopscience.iop.org/article/10.1088/0031-8949/45/5/013. doi:doi:10.1088/0031-8949/45/5/013.

[35] F. F. Chen, Introduction to Plasma Physics and Controlled Fusion, Springer US, Boston, MA, 1984. URL: http://link.springer.com/10.1007/978-1-4757-5595-4. doi:doi:10.1007/978-1-4757-5595-4.

[36] C. Calle, C. Buhler, M. Johansen, M. Hogue, S. Snyder, Active dust control and mitigation technology for lunar and martian exploration, Acta Astronautica 69 (2011) 1082–1088.

[37] G. Manju, T. K. Pant, P. Sreelatha, et al., Lunar near surface plasma environment from Chandrayaan-2 Lander platform: RAMBHA-LP payload, Current Science 118 (2020) 383–391. doi:doi:10.18520/cs/v118/i3/383-391.

[38] I. Kuznetsov, S. Hess, A. Zakharov, F. Cipriani, E. Seran, S. Popel, E. Lisin, O. Petrov, G. Dolnikov, A. Lyash, S. Kopnin, Numerical modelling of the Luna-Glob lander electric charging on the lunar surface with SPIS-DUST, Planetary and Space Science 156 (2018) 62–70. URL: https://linkinghub.elsevier.com/retrieve/pii/S0032063317302696. doi:doi:10.1016/j.pss.2018.03.004.

[39] N. Duncan, Z. Sternovsky, E. Gruen, S. Auer, M. Horanyi, K. Drake, J. Xie, G. Lawrence, D. Hansen, H. Le, The Electrostatic Lunar Dust Analyzer (ELDA) for the detection and trajectory measurement of slow-moving particles from the lunar surface, Planetary and Space Science (2011) 1446–1454. doi:doi:10.1016/j.pss.2011.06.002.

[40] G. Dolnikov, A. Kartasheva, A. Bychokova, I. SHashkova, I. Kuznetsov, A.N.Lyash, A. Dubov, S. Popel, A. Zakharov, Dusty plasm environment near lunar surface, in: XXXV International Conference on Equations of State for Matter, volume 1787, 2021, p. 012050.

[41] O. Hadjar, G. Johnson, J. Laskin, G. Kibelka, S. Shill, K. Kuhn, C. Cameron, S. Kassan, IonCCD for direct position-sensitive charged-particle detection: from electrons and kev ions to hyperthermal biomolecular ions, J. Am. Soc. Mass Spectrom. (2011).

[42] R. Fletcher, Electrostatic microprobe for determining charge domains on surfaces, Rev. Sci. Instrum. (2015).

[43] X. Wang, Z. Sternovsky, M. Horanyi, J. Deca, I. Garrick-Bethell, W. Farrell, J. Minafra, L. Bucciantini, Electrostatic Dust Analyzer (EDA) for charaterizing dust transport on the lunar surface, in: Lunar Surface Science Workshop, 5002, Lunar Planetary Institute, 2020.

[44] X. Wang, Z. Sternovsky, M. Horányi, The Dust BUSTER Team, Cubesat electrostatic dust analyzer (ceda) for measuring regolith dust transport on airless bodies, in: Proceedings of the AIAA/USU Conference on Small Satellites, 2018, pp. SSC18–WKVI–02.

[45] S. Kelz, T. Veigel, M. Groezing, M. Berroth, A fully differential charge-sensitive amplifier for dust-particle detectors, PRIME 2018, IEEE Conference Prague, Czech Republic (2018).

[46] G. Bertuccio, D. Macera, C. Graziani, M. Ahangarianabhari, A cmos charge sensitive amplifier with sub-electron equivalent noise charge, in: 2014 IEEE Nuclear Science Symposium and Medical Imaging Conference, 2014. doi:doi:10.1109/NSSMIC.2014.7431123.

[47] M. Hollick, B. J. O'Brien, Lunar weather measurements at three Apollo sites 1969-1976, Space Weather 11 (2013) 651–660.

[48] G. Heiken, D. McKay, R. Brown, Lunar deposits of possible pyroclastic origin, Geochim Cosmochim Acta 38 (1974) 1703–1704.

[49] J. Colwell, S. Batiste, M. Horanyi, S. Robertson, S. Sture, Lunar surface: Dust dynamics and regolith mechanics, Rev. Geophys. 45 (2007) RG2006.

[50] J. Kissel, K. Altwegg, B. C. Clark, L. Colangeli, H. Cottin, S. Czempiel, J. Eibl, C. Engrand, H. M. Fehringer, B. Feuerbacher, M. Fomenkova, A. Glasmachers, J. M. Greenberg, E. Grün, G. Haerendel, H. Henkel, M. Hilchenbach, H. Von Hoerner, H. Höfner, K. Hornung, E. K. Jessberger, A. Koch, H. Krüger, Y. Langevin, P. Parigger, F. Raulin, F. Rüdenauer, J. Rynö, E. R. Schmid, R. Schulz, J. Silén, W. Steiger, T. Stephan, L. Thirkell, R. Thomas, K. Torkar, N. G. Utterback, K. Varmuza, K. P. Wanczek, W. Werther, H. Zscheeg, Cosima - High resolution time-of-flight secondary ion mass spectrometer for the analysis of cometary dust particles onboard Rosetta, Space Science Reviews 128 (2007) 823–867. doi:doi:10.1007/s11214-006-9083-0.

[51] J. P. Bibring, P. Lamy, Y. Langevin, A. Soufflot, M. Berthé, J. Borg, F. Poulet, S. Mottola, Civa, Space Science Reviews 128 (2007) 397–412. doi:doi:10.1007/s11214-006-9135-5.

[52] J. E. McCoy, D. R. Criswell, Evidence for a high altitude distribution of lunar dust, Proceedings of the Fifth Lunar Conference (Supplement 5, Geochimica et Cosmochimica Acta), 1974, pp. 2991–3005.

[53] D. R. Criswell, Lunar dust motion, volume 3 of *Proceedings of the Third Lunar Science Conference (Supplement 3, Geochimica et Cosmochimica Acta)*, 1972, pp. 2671–2680.

[54] H. A. Zook, J. E. Mccoy, Large scale lunar horizon glow and a high altitude lunar dust exosphere, Geophysical Research Letters 18 (1991) 2117–2120.

[55] A. Poppe, M. Piquette, A. Likhanskii, M. Horányi, The effect of surface

topography on the lunar photoelectron sheath and electrostatic dust transport, Icarus 221 (2012) 135–146.

[56] S. Kameda, H. Suzuki, Y. Cho, et al., Detectability of hydrous minerals using ONC-T camera onboard the Hayabusa2 spacecraft, Advances in Space Research 56 (2015) 1,519–1,524. doi:doi:10.1016/j.asr.2015.06.037.

[57] S. Kameda, H. Suzuki, T. Takamatsu, et al., Preflight Calibration Test Results for Optical Navigation Camera Telescope (ONC-T) Onboard the Hayabusa2 Spacecraft, Space Science Review 208 (2017) 17–31. doi:doi:10.1007/s11214-015-0227-y.

[58] H. Suzuki, M. Yamada, T. Kouyama, et al., Initial inflight calibration for Hayabusa2 optical navigation camera (ONC) for science observations of asteroid Ryugu, Icarus 300 (2018) 341–359. doi:doi:10.1016/j.icarus.2017.09.011.

[59] E. Tatsumi, T. Kouyama, H. Suzuki, et al., Updated inflight calibration of Hayabusa2's optical navigation camera (ONC) for scientific observations during the cruise phase, Icarus 325 (2018) 153–195. doi:doi:10.1016/j.icarus.2019.01.015.

[60] R. Knollenberg, J. Gilland, IEEE Transactions on Geoscience and Remote Sensing GE-18 (1980) 100–104.

[61] D. A. Glenar, T. J. Stubbs, J. M. Hahn, Y. Wang, Search for a high-altitude lunar dust exosphere using Clementine navigational star tracker measurements, Journal of Geophysical Research: Planets 119 (2014) 2548–2567.

[62] R. Clegg-Watkins, B. Jolliff, A. Boyd, M. Robinson, R. Wagner, J. Stopar, J. Plescia, E. Speyerer, Photometric characterization of the Chang'e-3 landing site using LROC NAC images, Icarus 273 (2016) 84–95.

[63] J. E. Lane, P. T. Metzger, Estimation of Apollo lunar dust transport using optical extinction measurements, Acta Geophysica 63 (2015) 568–599.